Applications of a portable capillary electrophoresis instrument in environmental science

Inauguraldissertation

zur
Erlangung der Würde eines Doktors der Philosophie
vorgelegt der
Philosophisch-Naturwissenschaftlichen Fakultät
der Universität Basel

von
Natascha Torres
aus
Deutschland

Luzern, 2015

Genehmigt von der Philosophisch-Naturwissenschaftlichen Fakultät

auf Antrag von

Prof. Dr. Peter Hauser,

Prof. Dr. Christine Alewell

und

Dr. Beat Müller

Basel, den 23.06.2015

Prof. Dr. Jörg Schibler

Dekan

Acknowledgements

Ich hatte das grosse Glück von einzigartigen Persönlichkeiten mit interdisziplinärem Wissen begleitet zu werden. Ich danke jenen von ganzen Herzen für das entgegengebrachte Vertrauen, für grosszügige Freiheiten und viel Rückhalt. Diese vielseitige Unterstützung hat nicht nur dieses Projekt zum Erfolg geführt, sondern auch mich persönlich wachsen lassen.

Im Einzelnen gilt mein Dank meinem Doktorvater Prof. Peter Hauser, der mich in seinem Team aufnahm und mir das Projekt anvertraute. Mit kritischem Hinterfragen und konstruktiver Kritik motivierte er mich stets meine Arbeit zu reflektieren und zu verbessern.

Frau Prof. Christine Alewell danke ich für ihr Interesse und die Übernahme des Korreferates.

Dr. Beat Müller schulde ich grossen Dank. Einerseits für das Bereitstellen aller Ressourcen, aber noch vielmehr für die freundschaftliche Unterstützung, die er all die Jahre geleistet hat. Er half mir durch Zeiten des Zweifels, indem er unermüdlich an mich glaubte.

In Prof. Gerhard Furrer habe ich ein grosses Vorbild in Bezug auf Geduld und Sorgfalt gefunden. Ich glaube es war vor allem seine freigeistliche Haltung, die mich motivierte ein Projekt zu bearbeiten, dessen Ausgang so ungewiss war.

Prof. Helmut Brandl hat sich stets im richtigen Moment eingeschaltet. Er hat uns oft aus Diskussion geführt, die sich im Kreise drehten und uns wieder an den Fokus erinnert. Mit ihm verbinde ich, dass Wissenschaft vor allem grossen Spass macht und unkompliziert kommuniziert werden kann.

Mit Dr. Pavel Kubáň nahm diese Arbeit eine entscheidende Wende ein. Mit seiner Hilfe und Erfahrung brachten wir die sogenannte „Hardware“ endlich zum Funktionieren.

Mit Dr. Lawrence Och konnte ich viele spannende fachliche und persönliche Diskussionen über Wissenschaft und Leben führen, was mich oftmals wieder mit Enthusiasmus an die Arbeit zurück führte. Wann immer mich die Mutterschaft von der Forschung abhielt, ist er für mich eingesprungen.

Thomas Chwalek und Helen Droz-Georget danke ich vor allem für die unglaublich grosse Menge an Daten, die sie mir durch ihre Master-, bzw. Bachelorarbeit bereit gestellt haben.

Egal ob Sonderanfertigung spezieller Werkzeuge, Beratung von Messtechnik oder einfach nur ein Mitanpacken bei der Feldarbeit, ohne die Hilfe von Beat Kienholz und Michael Schurter wäre mir die Arbeit massgeblich schwerer gefallen.

Ruth Stierli und Patrick Kathriner waren die guten Seelen im Labor. Danke an die beiden für die vielen Messungen und analytischen Beratungen.

Auch das Team in Basel, namentlich Dr. Thanh Duc Mai, Dr. Marko Stojkovic, Dr. Hong Heng See und Benjamin Bomastyk, hat mich immer wieder mit Know-how und Technik unterstützt.

Doris Hohmann danke ich für die guten Gespräche und den Zugang zur Welt der Mikroben. Raffaele Leonetti hat mich immer sehr schnell und effizient in computertechnischen Angelegenheiten beraten und ist ein Meister im Troubleshooting.

Dr. Andreas Brand half mir die Grenzen der Wissenschaft besser zu ertragen. Brian Sinnet führte mich in die zauberhafte Welt der Rasterelektronenmikroskopie ein. Dr. Martin Ziegler eröffnete mir den Zugang zum Gesteinslabor, Monika Niederhuber und Daniel Trüssel ins GIS und Dr. Frederic Hammes in die ATP Analytik.

Nicht zu vergessen ist ein Dank an das Baikalteam: Dr. Michael Sturm, Dr. Elena Vologina, Prof. Nikolay Budnev und Prof. Eugene Sklyarov.

Dem Schweizerischen Nationalfond danke ich, in dieses Projekt investiert zu haben.

Ohne meine Freunde, die waren und die ich während der Zeit der Dissertation gewonnen habe, wäre ich nur halb so reich. Danke für die vergangenen und zukünftigen gemeinsamen Stunden.

Meine lieben Eltern und Grosseltern: Diese Arbeit steht auf eurem Fundament,- einer unbeschwerten Kindheit in Freiheit und Achtsamkeit.

Mein lieber Chisu, mein Sherpa: Danke, dass du mich begleitest, mich führst, mich trägst. Du bist mein allerbester Freund. Ich liebe Dich.

Meine beiden lieben Jungs: Ihr zwei Wunderwerke: Eure frohen Augen, eure strahlenden Gesichter, die kleinen feuchten Näschen. Dieses Werk ist in all jenen Stunden entstanden, in denen ich euch schmerzlich vermisst habe. Meine beiden Sonnen: Euer Strahlen wärmt mich, lässt mich wachsen, macht mich unendlich glücklich.

Summary

Capillary electrophoresis (CE) is a widely-used separation technique for the analysis of ionic species. It has crucial advantages due to high efficiencies given that small differences in ion mobility are often sufficient for the resolution. The key features of the CE instrument such as portability, rapidity of analysis and the need for only a small sample volume offer the potential to facilitate future work of environmental scientists. This thesis presents new applications of a portable CE instrument in the environment, including the associated sampling techniques and measurement protocols.

(i) A new method for the extraction and analysis of lake sediment pore water was developed. The extraction of the pore water from the sediment core was performed with filter tube samplers. Samples were immediately injected and measured by CE. All major cations and anions could be separated at once including the redox sensitive Fe(II) without any sample pretreatment. Along with fast injection, this prevents samples from alterations and contaminations. Sample volumes of only 20 µL allowed a high spatial resolution of the pore water profile, even with low water content.

(ii) In a next step, the new method was applied in the field at Lake Baikal. The CE instrument was thus carried by cabin luggage in the plane and assembled in improvised laboratory containers at the shore of the lake. The pore water analysis was performed immediately after coring. High-quality data enabled the explanation of the formation and transformation of very special iron (III) and manganese (IV) oxide layers, which are buried in the reducing part of the sediment. The analysis of Fe (II) and Mn (II) allowed the determination of sharp redox boundaries. Overall, the high-quality data from on-site measurement eliminated doubts concerning artefacts from previous measurements when core squeezing and sample pretreatment had to be practiced.

(iii) Besides the analysis of pore water, another challenging field in environmental science involves the surface analysis of rocks and biofilm. Thereby, surface processes are studied in terms of weathering, initial soil formation, as well as growth and vitality of microorganism. We developed a new method for the quantification of mobile ions and adenosine triphosphate (ATP) on surfaces. For the collection of available ions and ATP, a single drop of pure water was spread on the surface of the mineral or lichen and recollected for the analysis by CE and a luminometer, respectively. The heterogeneity of granites and the effect of wetting and freezing and thawing was shown on bare rock surfaces. On lichen, the effect of humidity and age on their vitality was demonstrated.

Contents

1 Introduction

1.1 Principles of capillary electrophoresis

1.1.1 Separation

Separation with capillary electrophoresis (CE) was first introduced by Tiselius in 1937 [1]. It is based on the different migration times of charged species in an electric field. The migration velocity v (cm/s) of the analytes depends on their electrophoretic velocity v_i and the electroosmotic velocity v_{EOF} of the electrolyte inside the capillary.

$$v = v_i + v_{EOF} \quad (1)$$

1.1.1.1 Electrophoretic mobility

The velocity v_i of the ions depends on the applied electric field E (V/cm) and the electrophoretic mobility μ_e (cm^2/Vs).

$$v_i = \mu_e E \quad (2)$$

The electric field E is a function of applied voltage and capillary length. The electrophoretic mobility μ_e depends on the electric and frictional forces the ion experiences.

The electric force F_e is given by the effective ion charge q and the applied electrical field E.

$$F_e = q E \quad (3)$$

The frictional force F_f for spherical ions is given by the solution viscosity η, the ion radius r and the ion velocity v_i.

$$F_f = -6 \pi \eta r v_i \quad (4)$$

The mobility μ_e thus can be described by

$$\mu_e = \frac{q}{6 \pi \eta r} \quad (5)$$

The parameters ***q*** and ***r*** in equation (5) indicate that small and highly charged ions are highly mobile, while large and minimally charged ions are less mobile.

1.1.1.2 Electroosmotic mobility

A fundamental process that drives CE is known as the electroosmotic flow (EOF) and it was first described by Helmholtz [2]. Many others [3-7] have further enhanced the model until present.

The EOF is caused by the interaction of the interior capillary wall with the ions of the electrolyte solution and thus depends on pH. Silanol groups (-SiOH) on silica capillary walls become deprotonated to silanolate groups ($-SiO^-$) if pH is above 4. The cations of the electrolyte solution will be attracted by the negatively charged ions on the capillary wall and form two inner layers of cations, a so-called diffuse double layer (Figure 1). The inner layer of cations is held to the negatively charged surface wall (fixed layer). This layer cannot neutralize the wall completely as the adsorption of the charged ions has insufficient density. Therefore, a second, mobile layer of cations is formed between the fixed layer and the electrolyte solution. By applying an electrical field, the mobile layer of cations is pulled to the cathode. These cations are surrounded by water molecules (solvated) and thus form hydrogen bonds to the molecules within the bulk solution. Thus, the bulk solution including cations and a variety of anions is swept towards the cathode.

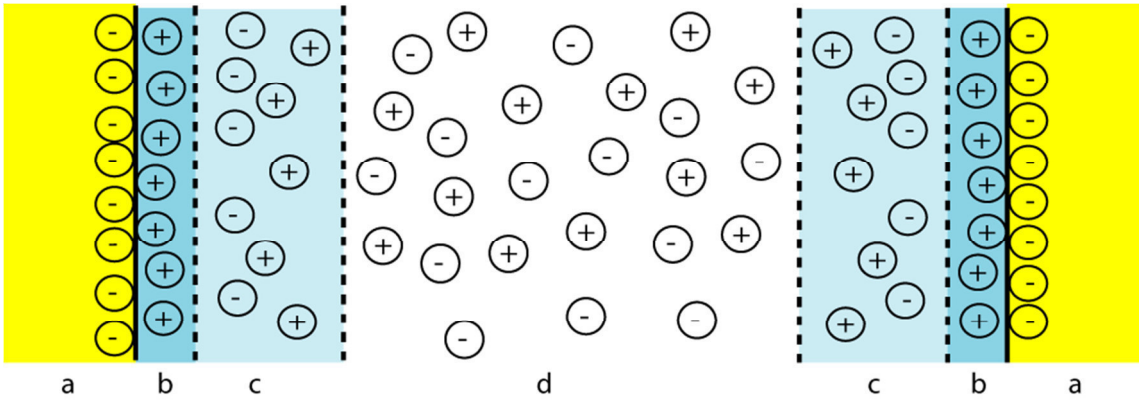

Figure 1: A cross section of a capillary showing a) the negatively charged capillary wall (yellow), b) a positively charged fixed layer, c) the diffuse layer and d) the bulk flow. The blue color indicates the diffuse double layer.

The driving force of the EOF is uniformly distributed within the capillary, which leads to a flat (rather than laminar) flow profile across the tubing diameter and narrow peaks (Figure 2).

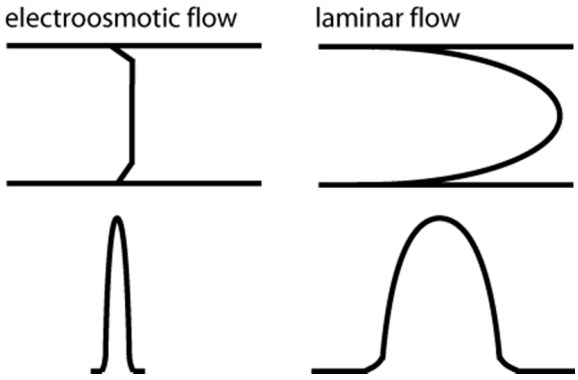

Figure 2: Flow profiles (above) and corresponding solute zones (below). Narrow flow profiles (left above) and corresponding sharp solute zones (left below) causing high efficiencies in detection. Small differences in migration velocity are sufficient for the resolution of analytes.

The velocity v_{EOF} of the EOF depends on its mobility μ_{EOF} and the applied electrical field E.

$$v_{EOF} = \mu_{EOF} E \qquad (6)$$

The mobility μ_{EOF} can be measured by using a neutral marker and it is proportional to the zeta-potential ζ and inversely proportional to the viscosity of the electrolyte η

$$\mu_{EOF} = \frac{lL}{Vt} \quad (7)$$

l = effective capillary length

L = total capillary length

V = electric field

t = migration time of EOF marker

$$\mu_{EOF} = \frac{\varepsilon_r \varepsilon_0 \zeta}{4 \pi \eta} \quad (8)$$

The zeta-potential ζ describes the electric imbalance between the fixed and mobile cation layers due to potential differences. ζ depends on the surface charge of the capillary wall σ, the thickness of the mobile layer δ and the dielectric constant ε_r of the electrolyte.

$$\zeta = \frac{4 \pi \sigma \delta}{\varepsilon_r \varepsilon_0} \quad (9)$$

$\varepsilon_0 = 8.854\ 10^{-12}$ As/Vm

The EOF plays a fundamental role in the analysis with CE, given that it causes the movement of cations and anions (with electrophoretic mobilities smaller than the magnitude of EOF) in the same direction. Anions and cations can be analyzed in a single run and in adequate time. Equation (8) indicates that the EOF is affected by many factors such as electrolyte viscosity, zeta-potential and the dielectric constant. These factors can be influenced by a number of parameters such as current, pH and concentration of the electrolyte or temperature. In addition, the inner surface charge of the capillary wall can be chemically modified with active reagents or ionic resins.

1.1.2 Efficiency and resolution

The efficiency determines the ability to separate or resolve solute zones and is limited by the degree of band broadening. Reasons for band broadening are molecular diffusion of the analytes, electrodispersion, Joule heating and interactions of the solutes with the capillary wall:

Molecular diffusion is defined by the diffusion coefficient of the analyte and decreases with its increasing molecular weight. Electrodispersion is caused by differences in sample zone and buffer conductivities. If the solute zone has a higher mobility than the buffer, the peak end will be diffuse (tailing) or, conversely, if the solute zone has a lower mobility than the buffer, the peak end will be very sharp while the beginning will be diffuse (leading) (Figure 3). Interactions of the solutes with the capillary wall can also lead to higher dispersion.

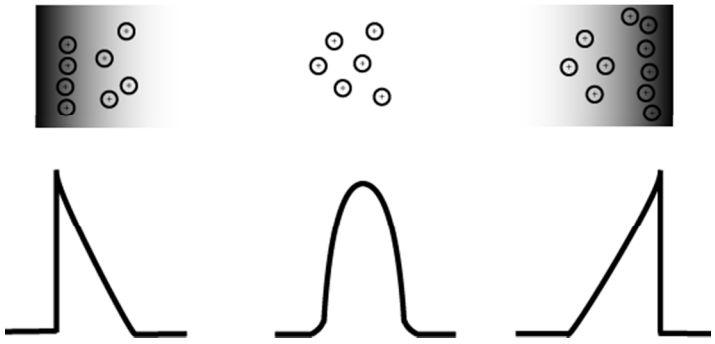

Figure 3: Electrodispersion caused by different mobilities in buffer solution and solute zone. Left: The solute zone moves slower than the buffer. Middle: The mobilities of buffer and solute zone are similar. Right: The solute zone moves faster than the buffer.

A further limiting factor is Joule heating, whereby the passage of the electrical current through the conductor generates temperature gradients inside the capillary. The dissipation of heat through the capillary wall leads to local changes in viscosity, causing laminar flow and thus zone broadening. Consequently, efficiency and resolution will be reduced.

The definition of efficiency and resolution in CE is adapted from chromatography.

To estimate efficiency it can be expressed as a theoretical plate number ***N***:

$$N = 5.54 \left(\frac{t}{w_{1/2}}\right)^2 \quad (10)$$

5.54 = to complete the Gaussian peak profile

t = migration time of the analyte

$w_{1/2}$ = peak width at half height

The full resolution ***R*** between two species is given by the equation:

$$R = \frac{2\,(t_2 - t_1)}{w1 + w2} \quad (11)$$

t = migration time

w = baseline peak width (in time)

Whether two peaks can be resolved from each other mainly depends on their migration times, concentration and the degree of band broadening.

1.1.3 Instrumentation

The overall simplicity of the instrument is a key feature of CE. A schematic diagram of a generic CE system shown in Figure 4, comprising a capillary, two reservoirs for the electrolyte background solution (buffer), a high voltage power supply, two electrodes and a detector. The ends of the capillary and the electrodes are placed in the buffer reservoir. The electrodes make the electric contact between the high voltage power supply and the capillary.

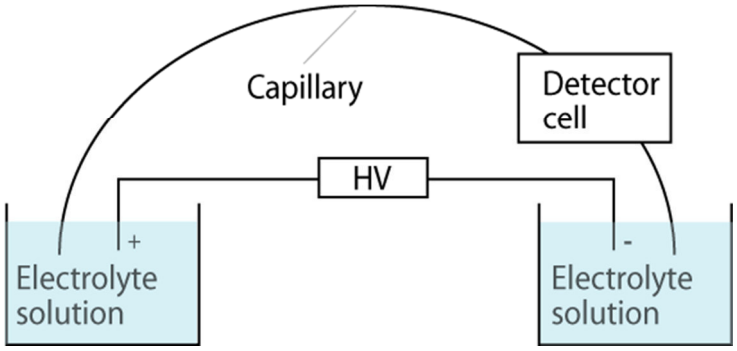

Figure 4: Basic parts of a capillary electrophoresis instrument.

To inject the sample into the capillary, the buffer reservoirs have to be replaced by the sample vial. A small amount of the sample (pico- to nanoliter) is loaded by applying pressure differences or an electrical field. The most common techniques are given in Figure 5. A simple method that is also applied in this study is the hydrodynamic injection. In this case, the flow of liquid is caused by the difference in pressure when one side of the capillary is lifted up to a certain level above the other (siphoning). The amount of the injected sample can be regulated by the height and duration of the lifting. After placing the capillary back from the sample vial to the buffer reservoir, the electric field is applied and the separation is performed.

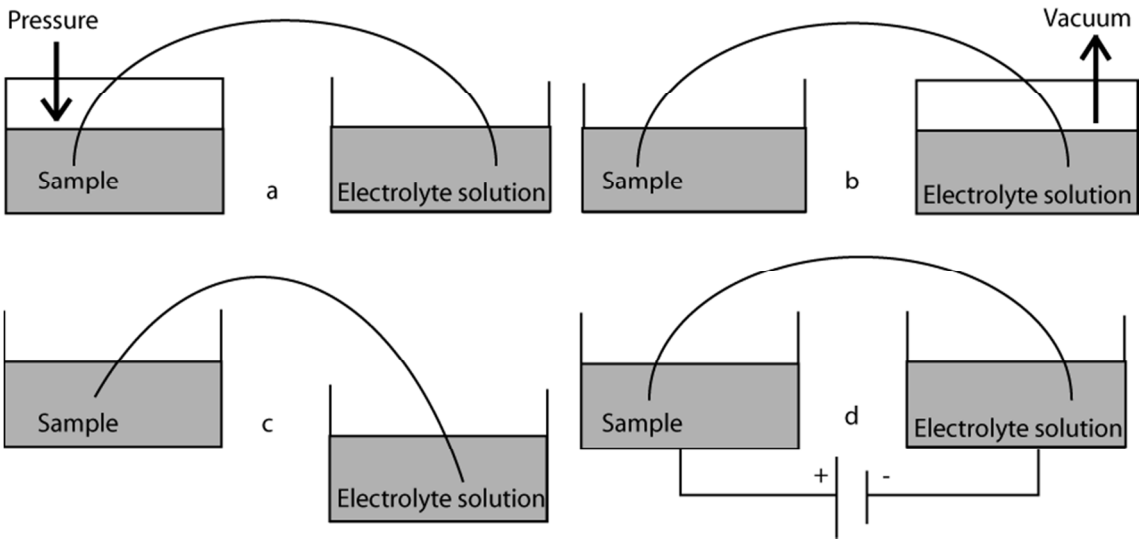

Figure 5: Common techniques for sample injection in CE. a) An external applied pressure injects the sample into the capillary; b) a vacuum at the end of the capillary causes aspiration; c) different height levels of the capillary cause aspiration of the sample due to differences in pressure; and d) an electrical field causes injection by electromigration.

The first prototypes of a CE system were constructed between 1958 and 1965 [8]. In 1967, a first instrument was designed for the separation of inorganic ions, proteins, nucleic acids and microorganisms [9]. Nevertheless, CE did not gain popular acceptance until the 1980s. Today, CE instruments are widely used for the analysis of ionic substances [8] in pharmaceutical, forensic and clinical applications or the food industry. Most of the benchtop CEs are equipped with UV/Vis absorbance, laser induced fluorescence and mass spectrometry detectors [10]. The portable CE instrument used in this study is shown in Figure 6. It was developed by Kubáň et al. [10] and it comprises a box with dimensions of 310 x 220 x 260 mm made from Perspex plates. Two handles were mounted to carry the apparatus. The high-voltage power supply is placed in an extra compartment on the back side of the box and the electronic control box to operate the current and voltage on the left side of the box. The left side of the box contains a tray for the background electrolyte solution. The right side separated by a Perspex plate contains another tray for the background electrolyte solution and a detector holder. The detection was carried out with a capacitively coupled contactless conductivity (C^4D) detector. An overview of detection in CE is provided in the next section.

Figure 6: Applying the CE instrument on-site.

1.1.4 Detection

Common detection techniques for CE are based on UV/Vis absorbance, laser-induced fluorescence and mass spectrometry, as well as electrochemical detection, including potentiometric, amperometric, and conductivity methods. The analysis of small ionic compounds was traditionally performed with optical detectors, as they were already available from HPLC. However, the detection limits were not adequate (> 5 µmol/L) and precision and accuracy was lower than in IC analysis [11]. Reasons for this included the short optical path of the fused-silica capillary as well as, high background noise caused by the addition of UV absorbents for the indirect detection of alkali and alkaline earth ions as they do not absorb UV-radiation.

Alternative detection methods - such as laser-induced fluorescence and electrochemical detection - have often been complex or fragile, involved high energy consumption or were only accessible for certain compounds [12]. However, small ions have high electrophoretic mobility and their corresponding conductivities would result in sensitive detection. Conductivity detectors are thus optimal although they were difficult to construct in small dimensions needed for capillaries with inner diameter ≤ 50 µm [13]. The sensing electrodes of

first conductivity detectors had been in contact with the electrolyte solution and were either placed in the separation field (on-column) or at short distance from the capillary end (end-column). The measuring and reference electrodes were placed in the same reservoir, which caused conflicts between separation voltage and electrochemical detection [14]. Furthermore, the sensing electrodes were difficult to mount and prone to fouling [15].

Small-sized and robust contactless detectors (CCD) were introduced in 1980 for isotachophoretic determination of inorganic and organic anions [16]. The detector cell was used for tubings of 800 µm outer and 450 µm inner diameter and could not been adapted for thin capillaries used in zone electrophoresis. In 1998 Fracassi da Silva and do Lago as well as Zemann et al. designed a capacitively coupled contactless conductivity detector (C^4D) for standard capillaries with two tubular electrodes [17,18]. The electrodes are placed outside and cylindrically around the capillary with a few mm detection gap in between, and form a capacitor with the electrolyte solution. Alternating current (ac-) voltage is applied to the first electrode, while the ac-current induced in the second electrode is measured, depending on the electric conductivity of the solution between the two electrodes (Figure 7). The detector cell is inexpensive and commercially available [19-21]. The combination of CE C^4D is a widely-used detection method for inorganic and organic species or biomolecules at present. However, the current challenge in advancing this technique concerns sampling and sample pretreatment [21].

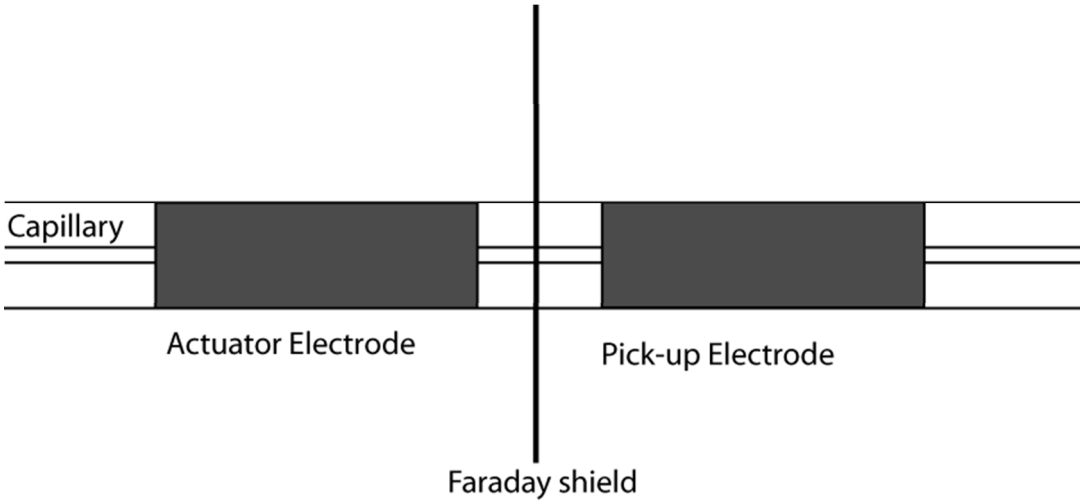

Figure 7: Schematic drawing of a C^4D. The capillary is axially wrapped by the electrodes.

1.2 Analysis of aqueous environmental samples

The analysis of environmental water is necessary to assess its physical-chemical, chemical or biological properties. The parameters are crucial for public health regulations, pollution control and to facilitate advantages in technology or policy decision-making [22].

Achieving representative data from the environmental water is generally challenging, given that chemical and biological reactions may destroy the analytes after the successful sample collection. Laborious pretreatment of the sample is required to preserve its integrity until measurement. Procedures include sample splitting for different analytical instruments or acidification to prevent precipitation. Therefore, immediate analysis of the sensitive compounds is essential and on-site methods are generally preferred.

Some parameters can be determined by field methods, e.g. dissolved oxygen and oxygen demand, pH, acidity and alkalinity, water hardness, and electrical conductivity. Common methods include conductivity measurements, colorimetric tests or ion sensitive electrodes. While portable laboratories for the on-site determination of some pollutants are commercially available, the quantification of the main inorganic constituents – such as SO_4^{2-}, Cl^-, NO_3^-, Ca^{2+}, Mg^{2+}, Na^+ , K^+ - is usually undertaken in the laboratory. The selection of the method depends on the expected concentration, the sample volume and number, as well as the time

and cost of the analysis [23]. The most widely-recommended techniques for the analysis of common ions are UV/Vis and atomic spectrometry (AAS, ICP-OES and ICP-MS), as well as IC. For instance, samples from lake water and lake sediment pore water have been routinely analyzed by IC in our group. In addition, NH_4^+, NO_3^-, SO_4^{2-} and orthophosphate has been determined with spectrophotometry if concentrations were too low for sufficient analysis by IC. The spectrophotometric analysis requires laborious sample pretreatment, e.g. the addition of agents to form light absorbing complexes with the analytes.

The data were used to study element cycling in natural waters and the physical, biogeochemical and microbial processes, as well as for water quality control. Depending on the concentration, compounds can be assessed as essential nutrients for organism, as well as pollutants. Familiar examples are nitrogen and phosphate used in fertilizers, which caused a serious eutrophication problem in many surface waters in the past.

1.3 Capillary electrophoresis for environmental applications

Capillary electrophoresis is a widely-used separation technique for the analysis of organic and inorganic ionic species. It has crucial advantages due to high efficiencies given that small differences in ion mobility are often sufficient for the resolution. Furthermore, CE requires a low volume of sample and reagents, is easily automated and can be applied to a wide selection of analytes. The instrumentation is simple and inexpensive. The control, suppress and adjustment of the EOF allows certain modes to run the CE with high degree of flexibility. Analysis by CE is routinely applied in the pharmaceutical, medical and food industries, as well as research to detect large organic molecules and biomolecules. This includes the detection and development of drugs, the measurement of urine and blood or the control of beverages [21].

The analysis of water samples with CE has been mainly described in low-income countries, e.g. for the assessment of drinking water from wells, taps or bottles [e.g. 24-27].

Nevertheless, CE was never recommended for routine water analysis by environmental authorities, given that the most commonly used UV absorption detectors have not reached adequate detection limits (~ 5 µmol/L) and thus IC and AAS remained the standard techniques [13,28]. At present, detection limits in CE are in a range of 0.1 -0.2 µmol/L for small inorganic ions with C^4D detectors [(reviews 19-21,29)]. The major inorganic ions from water can be simultaneously measured including a suite of trace metals [15,30]. However, detection limits of trace metals (1-5 µmol/L) were insufficient for the assessment of pollution and thus enrichment techniques have been developed [31].

CE has been applied to monitor heavy metal pollution, particularly arsenic and its compounds [32-34]. In addition to inorganic compounds, the assessment of organic pollutants from industry, households and agriculture has been more often reported in recent years. Some examples are phenols, surfactants, dyes, polycyclic aromatic hydrocarbons (PAHs), aromatic and aliphatic amines, aromatic acids and aromatic sulfonic acids and pesticides [35]. Furthermore, the detection of pollutants from pharmaceutical industries, antibiotics and remains from personal care products [36-39] have gained increasing importance in policy as they are harmful and hardly eliminated by waste water treatment plants.

1.4 Pore water analysis

Sediments from oceans and lakes are formed by particles settling from the water column and are important archives for the past. Their analysis allows assessing past environmental changes such as the effects of climate change and anthropogenic pollution [40-42]. The diagenetic processes - such as mineralization of organic matter, remobilization of nutrients, dissolution of particles, precipitation of secondary phases and adsorption [43] - control the reaction rates and transport of nutrients and trace elements. This dynamics are reflected in the concentration gradients of pore water. In general, the biochemical reactions are driven by the degradation of organic matter resulting in the gradual exhaustion of oxidants from the pore water. Macroscopically, associated redox processes are sequentially structured starting with the consumption of oxygen, denitrification, manganese oxide reduction, ferric oxide reduction and eventual methanogenesis [44]. A highly resolved characterization of the redox zones is thus important to understand the dynamics of processes. Concentration gradients of redox sensitive components in the pore water - such as NH_4^+, Mn(II), Fe(II), SO_4^{2-}, NO_3^- and CH_4 - indicate the rates of the redox reactions.

Although pore water reveal important information on early diagenesis, its analysis is still a challenge for oceanographers and limnologists. Key issues are fast and contamination-free sampling due to temperature and pressure changes inside the sediment cores, the conservation of the samples and their transport to the laboratory. Furthermore, the analysis of steep concentration gradients in the sediment demands for high spatial sampling resolution and thus analytical techniques that only need a minimum amount of sample volume.

Extracting pore water was first performed in the 1930s by digging holes into the sediment and collecting the seep water [45]. At present, the most widely-used techniques to separate interstitial water from sediments are squeezing devices, introduced by Reeburgh [46], as well as centrifugation, introduced by Edmunds and Bath [47]. Although both methods bear high risks for generating sample alteration due to oxidation and precipitation of compounds, they have

often been applied because of low-costs and easy handling. *In situ* measurements, e.g. diffusion plates [48] and microelectrodes [49] avoid temperature and pressure changes of the sediment, although they have long equilibration times or are only available for several species and the upper few cm of the sediment, respectively. Since 2005, filter tube samplers have been used to extract pore waters from an intact sediment core [50,51]. Although the sampling procedure is faster and less laborious, samples were still prone to alteration until measurement. In addition, the minimum sample volume needed for analysis is still > 100 µL, due to the standard instrument requirements and the fact that anions and cations could not have been measured from the same sample. The minimum sample volume has been often difficult to extract as pore water content decreases with increasing sediment depth. This study shows that the immediate injection of only a few microliter of sample for the analysis with CE can minimize many of the restrictions discussed above.

1.5 Surface analysis

Analytical methods for the quantification of bioavailable elements on organic and inorganic surfaces did not exist until present. Elements on surfaces have been generally determined by expensive techniques mainly based on microscopy or electron and mass spectrometry. For their investigation, the objects of interest often have to be removed from the original location and treated with coatings, whereby the surfaces were usually destroyed by the measurement. The fraction of mobile ions - e.g. to estimate weathering rates of rocks - were thus mainly indirectly measured by the concentrations of dissolved mineral constituents in runoffs [e.g. 52-54] or secondary phases in soil profiles [e.g. 55,56]. Changes in surface reactivity could thereby not be considered, although that controls the mineral degradation rate and thus the initial soil formation and its fertility [57]. This is known to be a precondition for the growth of organism and may influence the global climate [58]. Therefore, a technique to quantify bioavailable ions on rock and lichen surfaces was developed in this study.

1.6 Thesis outline

The remainder of this thesis is structured as follows, with a brief overview of each manuscript chapter detailed below. Chapters 2.1 and 2.2 have been published in Environmental Science Processes and Impacts in 2013 and 2014, respectively, while Chapter 2.3 was submitted to Chemical Geology in 2015.

Chapter 2.1: Sediment porewater extraction and analysis combining filter tube samplers and capillary electrophoresis

The measurement with the portable CE instrument was adapted for the analysis of lake sediment pore water. The combination with microporous filter tube samplers allowed the extraction of small sample volumes (< 20 µL) of pore water and thus a high spatial resolution of 5 mm. Due to immediate measurement with CE no conservation and transport was necessary. The risk of contamination was minimized as the samples were immediately injected for analysis without extra handling, such as splitting, acidification and dilution. The method was validated, comparing the results to those from IC of pore water samples from a eutrophic lake in Switzerland (Lake Baldegg). Major inorganic ions were successfully separated in less than 15 minutes. Due to fast injection and minimal disturbance of the pore water samples, zero-oxygen conditions were maintained, which allowed the analysis of oxygen-sensitive Fe(II). The time and effort of pore water sampling and measurement was thus reduced to a minimum. At the same time, the quality of the data was enhanced as the risk of alteration and contamination of the sample was reduced.

Chapter 2.2: Early diagenetic processes generate iron and manganese oxide layers in the sediments of Lake Baikal, Siberia

The method introduced in chapter 2.1 was applied on site on sediments from Lake Baikal. The pore water analysis was subsequently conducted after coring on site in improvised laboratory containers at the shore of the frozen lake. Accordingly, the geochemical processes leading to

the formation and dissolution of extraordinary buried iron- and manganese oxide layers in the reducing part of the sediment were explained with respect to the redox sequence. Due to the new approach, Fe(II) was detected and the iron reduction zone was precisely determined. It was demonstrated that the dissolution of the iron and manganese oxides is coupled to anaerobic oxidation of CH_4. Pathways are either directly coupled to the reduction of Fe (III) oxides or via the reduction of SO_4^{2-}, generating S(-II) which reduces the Fe (III) oxides. Moreover, concerns about artefacts resulting in the observed discontinuous NH_4^+ and the occurrence of NO_3^- in anoxic sediment were eliminated with the new technique. We discussed possible reasons for the persistence of NO_3^- and SO_4^{2-} in the methanogenic sediment zones, as well as for the burial of the Fe/Mn layers.

Chapter 2.3: A new method to quantify bioavailable elements and mobile ATP on rock surfaces and lichens

A new low-cost and non-destructive method for the on-site analysis of mobile ions and ATP on rock surfaces - either bare or overgrown with a biofilm - was developed. The mineral surfaces are subject to weathering, a prerequisite for colonization by microorganisms and initial soil formation. Given that their investigation is usually carried out under laboratory conditions using sophisticated instrumentation, the samples have to be removed and transferred. With the new method - called the DoR (Drop on Rock) method - cations, anions and ATP were collected in a drop of pure water previously spread onto the mineral surface. The analysis of dissolved ions and ATP in the recovered aqueous solution was carried out using a portable CE instrument and a luminometer, respectively. The methods were tested at surfaces of bare granite and crustose lichens. Some examples of potential applications of the DOR method are shown: the instant availability of nutrients on a bare granite surface depends on the local presence of the constituent minerals. Frost-thaw action in the initial state of exposition to harsh weather conditions did not enhance ion release. ATP - indicating the lichens' vitality - was found to be highly dependent on humidity and the age of the organism.

References

1 Tiselius, A. A new apparatus for electrophoretic analysis of colloidal mixtures. *Transactions of the Faraday Society* **33**, 524-531 (1937).

2 Helmholtz, H. Studien über electrische Grenzschichten. *Annalen der Physik* **243**, 337-382, doi:10.1002/andp.18792430702 (1879).

3 Gouy, M. Sur la constitution de la charge electrique a la surface d'un electrolyte. *Journal of Theoretical and Applied Physics* **9**, 457-468 (1910).

4 Chapman, D. L. LI. A contribution to the theory of electrocapillarity. *The London, Edinburgh, and Dublin Philosophical Magazine and Journal of Science* **25**, 475-481 (1913).

5 Stern, O. Zur theorie der elektrolytischen doppelschicht. *Zeitschrift für Elektrochemie und angewandte physikalische Chemie* **30**, 508-516 (1924).

6 Grahame, D. C. The electrical double layer and the theory of electrocapillarity. *Chemical Reviews* **41**, 441-501 (1947).

7 Bockris, J. M., Devanathan, M. & Muller, K. On the structure of charged interfaces. *Proceedings of the Royal Society of London. Series A. Mathematical and Physical Sciences* **274**, 55-79 (1963).

8 Fanali, S. *Handbook of capillary electrophoresis*. James P. Landers (Ed.), CRC Press Inc., 1996).

9 Hjertén, S. Free zone electrophoresis. *Chromatographic reviews* **9**, 122-219 (1967).

10 Kubáň, P., Nguyen, H. T. A., Macka, M., Haddad, P. R. & Hauser, P. C. New Fully Portable Instrument for the Versatile Determination of Cations and Anions by Capillary Electrophoresis with Contactless Conductivity Detection. *Electroanalysis* **19**, 2059-2065, doi:10.1002/elan.200703908 (2007).

11 Padarauskas, A. CE determination of small ions: methods and techniques. *Analytical and bioanalytical chemistry* **384**, 132-144 (2006).

12 Kubáň, P., Karlberg, B., Kubáň, P. & Kubáň, V. Application of a contactless conductometric detector for the simultaneous determination of small anions and cations by capillary electrophoresis with dual-opposite end injection. *Journal of Chromatography A* **964**, 227-241 (2002).

13 Zemann, A. J. Conductivity detection in capillary electrophoresis. *TrAC, Trends in Analytical Chemistry* **20**, 346-354, (2001).

14 Guijt, R. M., Evenhuis, C. J., Macka, M. & Haddad, P. R. Conductivity detection for conventional and miniaturised capillary electrophoresis systems. *Electrophoresis* **25**, 4032-4057 (2004).

15 Tanyanyiwa, J. & Hauser, P. C. High-voltage contactless conductivity detection of metal ions in capillary electrophoresis. *Electrophoresis* **23**, 3781-3786 (2002).

16 Gaš, B., Demjaněnko, M. & Vacik, J. High-frequency contactless conductivity detection in isotachophoresis. *Journal of Chromatography A* **192**, 253-257 (1980).

17 Fracassi da Silva, J. A. & do Lago, C. L. An Oscillometric Detector for Capillary Electrophoresis. *Analytical Chemistry* **70**, 4339-4343, doi:10.1021/ac980185g (1998).

18 Zemann, A. J., Schnell, E., Volgger, D. & Bonn, G. K. Contactless Conductivity Detection for Capillary Electrophoresis. *Analytical Chemistry* **70**, 563-567, doi:10.1021/ac9707592 (1998).

19 Kubáň, P. & Hauser, P. C. Ten years of axial capacitively coupled contactless conductivity detection for CZE–a review. *Electrophoresis* **30**, 176-188 (2009).

20 Kubáň, P. & Hauser, P. C. A review of the recent achievements in capacitively coupled contactless conductivity detection. *Analytica Chimica Acta* **607**, 15-29, doi:http://dx.doi.org/10.1016/j.aca.2007.11.045 (2008).

21 Kubáň, P. & Hauser, P. C. Contactless conductivity detection for analytical techniques—Developments from 2012 to 2014. *Electrophoresis* **36**, 195-211 (2015).

22 Keith, L. H. *et al.* Principles of environmental analysis. *Analytical Chemistry* **55**, 2210-2218, doi:10.1021/ac00264a003 (1983).

23 Radojevic, M. & Bashkin, V. N. *Practical environmental analysis*. (Royal Society of Chemistry, 1999).

24 Romano, J. P. & Krol, J. Capillary ion electrophoresis, an environmental method for the determination of anions in water. *Journal of Chromatography A* **640**, 403-412 (1993).

25 Oehrle, S. A. Analysis of anions in drinking water by capillary ion electrophoresis. *Journal of Chromatography A* **733**, 101-104 (1996).

26 Morin, P., Franclois, C. & Dreux, M. Capillary electrophoresis of alkali and alkaline-earth cations with imidazole or benzylamine buffers. *Journal of Liquid Chromatography & Related Technologies* **17**, 3869-3888 (1994).

27 Saad, B., Pok, F. W., Sujari, A. N. A. & Saleh, M. I. Analysis of anions and cations in drinking water samples by capillary ion analysis. *Food Chemistry* **61**, 249-254 (1998).

28 Haumann, I., Boden, J., Mainka, A. & Jegle, U. Simultaneous determination of inorganic anions and cations by capillary electrophoresis with indirect UV detection. *Journal of Chromatography A* **895**, 269-277, doi:http://dx.doi.org/10.1016/S0021-9673(00)00667-1 (2000).

29 Elbashir, A. A. & Aboul-Enein, H. Y. Recent applications and developments of capacitively coupled contactless conductivity detection (CE-C4D) in capillary electrophoresis. *Biomedical Chromatography* **28**, 1502-1506 (2014).

30 Kubáň, P., Kubáň, P. & Kubáň, V. Simultaneous determination of inorganic and organic anions, alkali, alkaline earth and transition metal cations by capillary electrophoresis with contactless conductometric detection. *Electrophoresis* **23**, 3725-3734 (2002).

31 Wen, Y., Li, J., Ma, J. & Chen, L. Recent advances in enrichment techniques for trace analysis in capillary electrophoresis. *Electrophoresis* **33**, 2933-2952 (2012).

32 Nguyen, H. T. A., Kubáň, P., Pham, V. H. & Hauser, P. C. Study of the determination of inorganic arsenic species by CE with capacitively coupled contactless conductivity detection. *Electrophoresis* **28**, 3500-3506 (2007).

33 Leermakers, M. *et al.* Toxic arsenic compounds in environmental samples: Speciation and validation. *TrAC, Trends in Analytical Chemistry* **25**, 1-10 (2006).

34 Melamed, D. Monitoring arsenic in the environment: a review of science and technologies with the potential for field measurements. *Analytica Chimica Acta* **532**, 1-13 (2005).

35 Martínez, D., Cugat, M. J., Borrull, F. & Calull, M. Solid-phase extraction coupling to capillary electrophoresis with emphasis on environmental analysis. *Journal of Chromatography A* **902**, 65-89, doi:http://dx.doi.org/10.1016/S0021-9673(00)00839-6 (2000).

36 Bailón-Pérez, M., Garcia-Campana, A., Cruces-Blanco, C. & del Olmo Iruela, M. Trace determination of β-lactam antibiotics in environmental aqueous samples using

off-line and on-line preconcentration in capillary electrophoresis. *Journal of Chromatography A* **1185**, 273-280 (2008).

37 García-Campaña, A. M., Gámiz-Gracia, L., Lara, F. J., del Olmo Iruela, M. & Cruces-Blanco, C. Applications of capillary electrophoresis to the determination of antibiotics in food and environmental samples. *Analytical and bioanalytical chemistry* **395**, 967-986 (2009).

38 Himmelsbach, M., Buchberger, W. & Klampfl, C. W. Determination of antidepressants in surface and waste water samples by capillary electrophoresis with electrospray ionization mass spectrometric detection after preconcentration using off-line solid-phase extraction. *Electrophoresis* **27**, 1220-1226 (2006).

39 Gibbons, S. E., Wang, C. & Ma, Y. Determination of pharmaceutical and personal care products in wastewater by capillary electrophoresis with UV detection. *Talanta* **84**, 1163-1168 (2011).

40 Chapman, P. M., Wang, F., Germano, J. D. & Batley, G. Pore water testing and analysis: the good, the bad, and the ugly. *Marine Pollution Bulletin* **44**, 359-366, doi:http://dx.doi.org/10.1016/S0025-326X(01)00243-0 (2002).

41 Winger, P., Lasier, P. & Jackson, B. The influence of extraction procedure on ion concentrations in sediment pore water. *Archives of environmental contamination and toxicology* **35**, 8-13 (1998).

42 Bufflap, S. E. & Allen, H. E. Sediment pore water collection methods for trace metal analysis: A review. *Water Research* **29**, 165-177, doi:http://dx.doi.org/10.1016/0043-1354(94)E0105-F (1995).

43 Berner, R. A. *Early diagenesis: A theoretical approach*. (Princeton University Press, 1980).

44 Froelich, P. N. *et al.* Early oxidation of organic matter in pelagic sediments of the eastern equatorial Atlantic: suboxic diagenesis. *Geochimica et Cosmochimica Acta* **43**, 1075-1090, doi:10.1016/0016-7037(79)90095-4 (1979).

45 Reid, D. M. Salinity Interchange between Salt Water in Sand and Overflowing Fresh Water at Low Tide. II. *Journal of the Marine Biological Association of the United Kingdom (New Series)* **18**, 299-306, doi:doi:10.1017/S002531540005150X (1932).

46 Reeburgh, W. S. An improved interstitial water sampler. *Limnology and Oceanography* **12**, 163-165, doi:10.4319/lo.1967.12.1.0163 (1967).

47 Edmunds, W. M. & Bath, A. H. Centrifuge extraction and chemical analysis of interstitial waters. *Environmental Science & Technology* **10**, 467-472 (1976).

48 Hesslein, R. H. An in situ sampler for close interval pore water studies1. *Limnology and Oceanography* **21**, 912-914 (1976).

49 Luther, G. W., Reimers, C. E., Nuzzio, D. B. & Lovalvo, D. In situ deployment of voltammetric, potentiometric, and amperometric microelectrodes from a ROV to determine dissolved O2, Mn, Fe, S (-2), and pH in porewaters. *Environmental Science & Technology* **33**, 4352-4356 (1999).

50 Seeberg-Elverfeldt, J., Schlüter, M., Feseker, T. & Kölling, M. Rhizon sampling of porewaters near the sediment-water interface of aquatic systems. *Limnology and oceanography: Methods* **3**, 361-371 (2005).

51 Shotbolt, L. Pore water sampling from lake and estuary sediments using Rhizon samplers. *Journal of Paleolimnology* **44**, 695-700 (2010).

52 White, A. F. & Brantley, S. L. Chemical weathering rates of silicate minerals: an overview. *Chemical Weathering Rates of Silicate Minerals* **31**, 1-22 (1995).

53 Hosein, R., Arn, K., Steinmann, P. & Adatte, T. Carbonate and silicate weathering in two presently glaciated, crystalline catchments in the Swiss Alps. *Geochimica et Cosmochimica Acta* **68**, 1021-1033 (2004).

54 Anderson, S. P. Glaciers show direct linkage between erosion rate and chemical weathering fluxes. *Geomorphology* **67**, 147-157 (2005).

55 Egli, M., Mirabella, A., Sartori, G. & Fitze, P. Weathering rates as a function of climate: results from a climosequence of the Val Genova (Trentino, Italian Alps). *Geoderma* **111**, 99-121 (2003).

56 Chadwick, O. A., Brimhall, G. H. & Hendricks, D. M. From a black to a gray box—a mass balance interpretation of pedogenesis. *Geomorphology* **3**, 369-390 (1990).

57 Flemming, H.-C. & Wingender, J. The biofilm matrix. *Nature Reviews Microbiology* **8**, 623-633 (2010).

58 Paytan, A. Mountains, Weathering, and Climate. *Science* **335**, 810-811 (2012).

2 Results and Discussion

2.1 Sediment porewater extraction and analysis combining filter tube samplers and capillary electrophoresis

Environ Sci Process Impacts. 2013 Apr;15(4):715-20. doi: 10.1039/c3em00068k.

Environmental Science
Processes & Impacts

Formerly Journal of Environmental Monitoring

http://rsc.li/process-impacts

Volume 15 | Number 4 | April 2013 | Pages 693–888

ISSN 2050-7887

RSC Publishing

PAPER

Beat Müller *et al.*

Sediment porewater extraction and analysis combining filter tube samplers and capillary electrophoresis

2050-7887(2013)15:4;1-X

Environmental Science
Processes & Impacts

RSC Publishing

PAPER

Sediment porewater extraction and analysis combining filter tube samplers and capillary electrophoresis

Cite this: *Environ. Sci.: Processes Impacts*, 2013, **15**, 715

Natascha T. Torres,[ab] Peter C. Hauser,[b] Gerhard Furrer,[c] Helmut Brandl[d] and Beat Müller*[a]

Careful extraction and analysis of porewater from sediment cores are critical for the investigation of small-scale biogeochemical processes. Firstly, small sample volumes and high spatial resolution are required. Secondly, several chemical species in the anaerobic porewater are sensitive to oxidation when brought in contact with ambient air. Here we present the combination of a special sampling technique and an analytical method for the porewater extraction of a varved sediment core from Lake Baldegg in central Switzerland, using MicroRhizon samplers and a portable capillary electrophoresis (CE) instrument. MicroRhizon filter tubes of 1 mm diameter and 20 mm length are suitable for fast retrieval of particle-free porewater samples directly from the sediment core. Since the time-span between sampling and analysis is less than 20 seconds, oxygen-sensitive Fe(II) can be analyzed in one go together with Na^+, K^+, Ca^{2+}, Mg^{2+}, NH_4^+, and Mn(II) without splitting, acidification or dilution of the sample. The major inorganic cations and anions of the sediment porewater can be determined in less than 15 minutes. Detection limits are in the sub-micromolar concentration range. The capillary electrophoresis instrument used in this study requires sample volumes of only 20 μL. These remarkable small sample volumes allow the minimization of disturbance of the sediment cores and a high spatial resolution of the sediment profile, even in sediments with low water content. The equipment is inexpensive, easy to handle, fully portable and therefore suitable for environmental on-site applications.

Received 4th February 2013
Accepted 20th February 2013

DOI: 10.1039/c3em00068k

rsc.li/process-impacts

Environmental impact

Early diagenetic processes in lake sediments can be traced and quantified from porewater concentration gradients. Exemplified for the sediments of Lake Baldegg (Switzerland), a eutrophic lake whose sediment oxygen consumption rate remained unchanged despite significantly decreased phosphate concentrations, we demonstrate the advantages of a new combination of porewater extraction and subsequent analysis of inorganic cations and anions. Remarkably small sample volumes are collected with minimal disturbance of the sediment and immediately analyzed without any pretreatments steps. The procedure allows high sample throughput and spatial resolution with a short time-span between sampling and analysis allowing the determination of oxygen-sensitive Fe(II) together with the major inorganic ions.

1 Introduction

The extraction and analysis of porewater from sediments are some of the most important techniques for the investigation of small scale biogeochemical processes and cycles, *e.g.* for the estimation of fluxes from and to the sediment–water interface, quantification of burial and mineralization rates of organic matter and production rates of climate affecting methane, or for quality assessments to estimate chemical contamination and toxicity.[1,2] Because of the high sensitivity of porewaters to changes in pressure, temperature, and redox potential, suitable extraction techniques are essential. They should be easy to use, avoid contamination risks, and provide sufficient vertical resolution as well as a good porewater yield at high throughput. Artefacts such as sorption/desorption processes or cell lysis should be avoided. For remote areas it is important to have lightweight and simple equipment. In general, on-site methods are to be preferred because the long transport of the sediments can cause temperature changes, outgassing due to decompression, mixing, diffusion, and redox changes at the sediment–water interface.

Since the 1960s porewater extraction techniques have been improved with regard to simplicity, rapidity, spatial resolution, and integrity of the sediments. The most widely used methods are, because of easy handling and inexpensiveness, *ex situ*

[a]*Eawag, Swiss Federal Institute of Aquatic Science and Technology, CH-6047 Kastanienbaum, Switzerland. E-mail: beat.mueller@eawag.ch; natascha.torres@eawag.ch*

[b]*Department of Chemistry, University of Basel, CH-4056 Basel, Switzerland*

[c]*Institute of Biogeochemistry and Pollution Dynamics, ETH Zurich, CH-8092 Zurich, Switzerland*

[d]*Institute of Evolutionary Biology and Environmental Studies, University of Zurich, CH-8057 Zurich, Switzerland*

techniques including squeezing and centrifugation[3] of the sediment. The squeezing methods are classified into core section squeezers[4–6] and whole core squeezers.[7,8]

Centrifugation is widely used but requires subsequent filtration to remove remaining suspended particles.[1] Moreover, it is difficult to avoid contact with ambient air. To minimize sampling artefacts such as chemical alterations of the porewater induced by oxygen, temperature changes and decompression,[1] *in situ* sampling techniques, like diffusion plates ("peepers") were introduced by Hesslein[9] and refined for the two-dimensional mapping of sediment sections by Lewandowski *et al.*[10] Peepers rely on the passive diffusion of dissolved compounds from the porewater across a filter membrane into compartments filled with distilled water.[11] For the improvement of equilibration time, a gel sampler[12] was developed, which reduced the required exposition time from days to hours. Profiling the sediment–water interface with ion-selective electrodes allowed the measurement of porewater concentration gradients with a spatial resolution of around 25 μm, but were only available for the detection of particular ions in the top few centimeters.[13–15]

Many of these limitations (artefacts with *ex situ* methods on the one hand and difficult handling with *in situ* methods on the other hand) can be overcome by using MicroRhizons (Rhizosphere Research Products, Wageningen), for porewater extraction. The MicroRhizons consist of a microporous polymer tube of 0.15 μm pore size[16] and a PEEK tubing, which can be connected to a syringe. A vacuum can be applied by a peristaltic pump or a syringe. Only a few authors[2,17,18] used this technology, which was originally designed for soil science to collect seepage water, despite the fact that this material is chemically inert and without ion exchange properties, permeable only for liquids, durable, fast, easy to use, inexpensive and reusable after rinsing.[19–21] Seeberg-Elverfeldt *et al.*[2] showed with tracer experiments and numerical modeling that approximately 2 mL sample volumes can be extracted attaining a resolution of ~1 cm even with low sediment porosities. Short-term processes can be investigated because of the fast and easy sampling procedure. The contamination with oxygen is minimal and anaerobic sampling does not require the installation of a glove box.[17] Despite the many advantages of the method, however, sample handling and analysis remain a challenge due to the small volume, the need for splitting and preservation, and the risk of contamination.[14,22] Field-portable instrumentation can overcome these problems by the immediate analysis of the extracted sample.[23–25] Therefore, a combination of MicroRhizons and a portable capillary electrophoresis (CE) instrument is ideal. Only a few microliters of sample volumes are needed and the analysis can be carried out on-site.

Kubáň *et al.*[26] developed and optimized a portable capillary electrophoresis instrument with capacitively coupled contactless conductivity detection (C^4D)[27] for the sensitive field measurements of ionic compounds in environmental samples. Inorganic ions could be determined with detection limits in the range of ~0.2 to 1 μM. CE can be implemented in lightweight portable equipment as only a separation capillary, a high voltage power supply, and small volumes of buffer solutions are needed. The very small and contact free detector system requires a data acquisition system connected to a laptop computer for immediate data storage and processing.[28] Only tiny water volumes (<20 μL) are required for analysis. The CE instrument with C^4D has been successfully tested in several environmental applications, *e.g.* the determination of major inorganic cations and anions in natural waters.[26,28,29]

Here we present an application for porewater sampling and analysis combining MicroRhizon samplers and a portable CE instrument. The facility combines the advantages of fast sampling with minimal bias and high spatial resolution and coincidentally the analysis of extremely small volumes and portability. The design and performance of the method is presented and exemplified with sediment cores from a eutrophic lake in Switzerland where porewater concentration measurements were compared with simultaneous analysis by ion chromatography (IC).

2 Experimental

2.1 Sampling site and sediment coring

Sediment cores were sampled from the deepest location (66 m) of Lake Baldegg, a eutrophic lake in central Switzerland of 5.2 km^2 surface area which has been artificially aerated since 1982 (geographic position: Lat 47°11.907′, Lng 8°15.590′).[30] The sediments of Lake Baldegg are varved as a consequence of anaerobic deep water since 1885[31] caused by the discharge of nutrients from household sewage, and intensified agriculture. Cores for the measurements of anions and cations were collected in April and June 2012, respectively, using a Uwitec gravity corer (www.uwitec.at). The tube of 65 cm diameter and 60 cm length was made of PVC and holes of 0.1 cm diameter were drilled staggered with a vertical resolution of 0.5 cm. The holes were sealed with a tape before coring. For the retrieval of porewater the tapes covering the sampling holes were cut open with a paper knife. A MicroRhizon sampler (Rhizosphere Research Products, Wageningen, Netherlands) of 2 cm length and 1 mm diameter connected to a 1 mL syringe was inserted horizontally and 10 to 50 μL of porewater were drawn out gently. The MicroRhizon sampler consists of a hydrophilic membrane (composed of a blend of polyvinylpyrrolidine and polyethersulfone) of 0.15–0.20 μm pore size. Sampling of one location takes less than 30 seconds. For the present experiments relatively large porewater volumes of 50 to 100 μL were collected until a 5.5 cm depth to allow verification of the CE data by IC measurements. Otherwise, the retrieval of 10 μL was sufficient for determinations with CE. The extracted porewater samples were transferred to 1 mL PE centrifugation tubes and immediately injected into the capillary for the CE measurement. Blanks (Nanopure water collected with MicroRhizon samplers) and certified multielement ion chromatography standard solutions (Fluka, Buchs, Switzerland) were intermittently measured to ensure a high data quality. All samples were stored at 5 °C in the dark for subsequent analysis with IC.

2.2 Apparatus and procedures

The determination of cations and anions was carried out using a portable capillary electrophoresis (CE) instrument with

capacitively coupled contactless conductivity detection (C^4D). The instrument was a modification of the model developed by Kubáň *et al.*[26] A sketch is given in Fig. 1. It consists of a box with dimensions of 310 × 220 × 260 mm made of Perspex plates, which can be opened at the front. The left side contains the sample and the vial holder, and the right side, separated by a Perspex plate, a vial holder and the detector holder. The high voltage supply from Spellman High Voltage Electronics Corporation, New York, was attached to the back, and the purpose-made electronic controller was fixed at the left side of the box.

A TraceDec® C^4D detector (Innovative Sensor Technologies GmbH, Strasshof, Austria) was used and the signal was recorded with the Tracemon software application. The peaks were analyzed using the Chart Software (version 5.2) from eDAQ, Australia. A fused silica capillary (50 μm i.d., 360 μm o.d., 55 cm length) (BGB Analytik AG, Böckten, Switzerland) was used for the separation. The capillary was preconditioned with 1 M NaOH for 5 minutes, rinsed with Nanopure water for 5 minutes and 1 M HCl for 5 minutes, rinsed with Nanopure water for 5 minutes, and finally equilibrated with the electrolyte solution for at least 30 minutes. A voltage of 15 kV was applied to the buffer vials at both ends of the capillary. The polarity of the applied separation voltage could be set by a switch, depending on whether anions or cations were recorded. The sample was injected hydrodynamically by elevating the capillary end immersed in the sample vial. Best results were obtained for an injection time of 20 seconds at 15 cm height for anions and 8 cm for cations. The detector settings were as follows. Frequency: 2× high, voltage level: 0 dB, gain: 200%, offset: 185. The electrolyte solution for both, the separation of cations as well as anions, consisted of 11 mmol L^{-1} L-histidine, 50 mmol L^{-1} acetic acid, 1.5 mmol L^{-1} 18-crown-6 and 0.1 mmol L^{-1} citric acid.[26] All solutions were ultrasonicated for 30 minutes. Chemicals were of p. a. grade (purchased from Sigma-Aldrich, Steinheim, Germany, or from Fluka, Buchs, Switzerland) and only used with Nanopure water purified on a Purelab Ultra (ElGA LabWater, UK). The stock solutions of cations were prepared immediately before use from the corresponding chloride salts, except of the ferrous iron stock solution, which was prepared from its sulfate salt. The stock solutions of anions were prepared from the corresponding sodium or potassium salts. The multi-ion standard solutions for the calibration were freshly prepared from these stock solutions. Cation standard solutions were prepared in 10^{-4} M HCl (suprapure). The concentration range of the standards was adjusted to the range expected for the sediment porewater samples (Table 1).

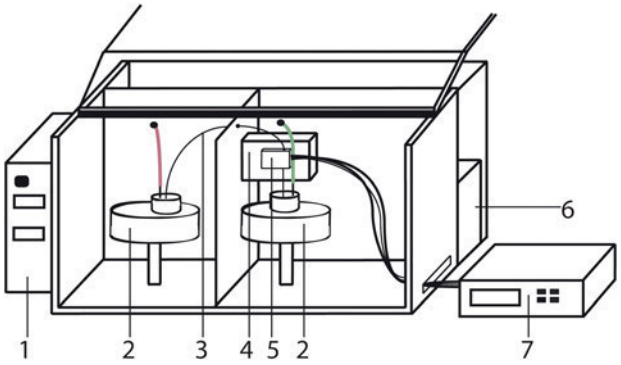

Fig. 1 Sketch of the portable capillary electrophoresis instrument with a C^4D detector. (1) Electronic control box, (2) buffer vial holder, (3) capillary, (4) detector cell holder, (5) detector cell, (6) Spellman High Voltage power supply, and (7) detector.

Table 1 Concentrations of standards (STc) for the calibration of the instrument adapted to the concentration ranges in the sediment porewater of Lake Baldegg

Ions	Blank, μmol L^{-1}	STc 1, μmol L^{-1}	STc 2, μmol L^{-1}	STc 3, μmol L^{-1}	STc 4, μmol L^{-1}
NH_4^+	0	70	100	200	500
K^+	0	17.5	25	50	125
Ca^{2+}	0	140	200	400	1000
Na^+	0	70	100	200	500
Mg^{2+}	0	70	100	200	500
Mn^{2+}	0	17.5	25	50	125
Fe^{2+}	0	50	150	300	600
Cl^-	0	25	50	100	—
NO_3^-	0	25	50	100	—
SO_4^{2-}	0	25	50	100	—
DIP	0	25	50	100	—

Samples, extracted from 0 until 5.5 cm core depth, were additionally measured by IC (Metrohm, Switzerland). NH_4^+, Na^+, K^+, Ca^{2+}, Mg^{2+} and Mn^{2+} were determined with a Metrosep C4 100/4.0 column (eluent: 1.7 mmol L^{-1} nitric acid, 0.7 mmol L^{-1} dipicolinic acid, flow: 0.9 mL min^{-1}). Cl^-, NO_3^- and SO_4^{2-} were determined with a Metrosep A Supp 5 column (eluent: 3.2 mmol L^{-1} Na_2CO_3, 1.0 mmol L^{-1} $NaHCO_3$, flow: 0.7 mL min^{-1}). The concentrations of dissolved inorganic phosphorus (DIP) and Fe^{2+} ions were not determined with IC, because acidification would be necessary to avoid oxidation and precipitation. The sample volume obtained by the MicroRhizons was too small for an accurate dilution with acid.

3 Results and discussion

3.1 Performance and validation of CE measurements

The analysis of the entire core was accomplished within less than five hours after coring. Electropherograms from the analysis of sediment porewater concentrations of cations and anions are shown in Fig. 2. All peaks could be fully resolved in undiluted samples. The amount injected was optimized in order to allow this resolution while still providing the required sensitivity. For the cations, a high sensitivity was required to allow the determination of K^+, which was present at a low concentration, but at the same time a signal overlap with Ca^{2+}, the ion with the highest concentration, had to be avoided. Results were at an optimum for an injection time of 20 seconds at 8 cm height for cations and at 15 cm height for anions (hydrodynamic injection by syphoning). Inorganic cations of the sediment porewater, Na^+, K^+, Ca^{2+}, Mg^{2+}, NH_4^+ including Mn(II) and Fe(II), could be analyzed in less than six minutes. Anions (Cl^-, NO_3^-, SO_4^{2-}, DIP) were analyzed in less than ten minutes (Cl^-, NO_3^-, SO_4^{2-} in less than five minutes).

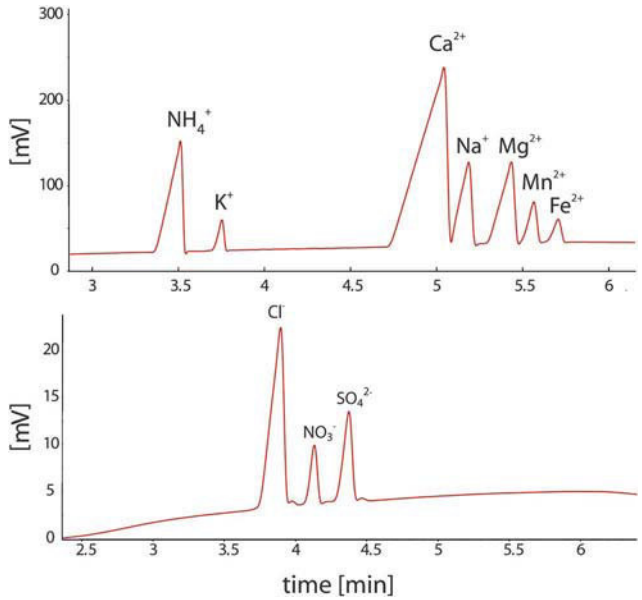

Fig. 2 Determination of cations (sample from a 15 cm sediment depth) and anions (sample at the sediment–water interface) from the Lake Baldegg sediment porewater. The concentrations were 700 μmol L^{-1} NH_4^+, 100 μmol L^{-1} K^+, 1500 μmol L^{-1} Ca^{2+}, 500 μmol L^{-1} Na^+, 320 μmol L^{-1} Mg^{2+}, 120 μmol L^{-1} Mn^{2+}, and 70 μmol L^{-1} Fe^{2+} for the cations and 610 μmol L^{-1} Cl^-, 120 μmol L^{-1} NO_3^-, and 120 μmol L^{-1} SO_4^{2-} for the anions.

Lines of best fit and coefficient values were determined based on four to five-point calibrations in the expected concentration range (Table 2). All calibration functions were very reproducible over time, and intercepts were close to zero. Slopes of five calibration functions recorded on different days in September 2012 varied only by 6%, even without thermostating of the detector cell. The limits of detection (LOD) are in the sub-micromolar range and were determined corresponding to a three times signal to noise ratio ($3 \times S/N$).

The CE instrumentation has a number of advantages such as the possibility to detect a large set of cations and anions within minutes, requiring negligible sample volumes. The determinations are highly reproducible with low detection limits, and the equipment is inexpensive and lightweight. These characteristics and the portability of the measuring device are important, *e.g.* in the analysis of sediment porewaters requiring fast sampling of only small volumes and the sensitive measurement of as many compounds as possible avoiding dilution and preservation of samples. A representative application to freshwater sediment porewater analysis in combination with a fast and easy sampling principle is presented in the following section.

Table 2 Analytical parameters for the determination of inorganic ions. The relative standard deviation (RSD) was calculated from peak areas of standard solutions used for the calibration of the porewater samples (Table 1). Each standard solution was measured three times. The correlation coefficients, r^2, were obtained for the corresponding calibration curves. The limits of detection (LOD) were defined as three-fold of the signal/noise ratio ($3 \times S/N$)

Ion	RSD (%), peak area	r^2, peak area	LOD, μmol L^{-1}
NH_4^+	2.43	0.998	0.46
K^+	2.20	0.997	0.76
Ca^{2+}	1.32	0.994	0.47
Na^+	3.25	0.997	0.79
Mg^{2+}	2.72	0.998	0.53
Mn^{2+}	3.22	0.996	0.82
Fe^{2+}	2.47	0.998	1.55
Cl^-	4.79	0.982	0.98
NO_3^-	3.23	0.997	0.29
SO_4^{2-}	1.37	0.999	0.28
DIP	7.80	0.988	0.83

3.2 Lake sediment porewater sampling and analysis applying MicroRhizons and CE

Fig. 3 depicts porewater concentrations of cations and anions from sediment cores of Lake Baldegg sampled with MicroRhizon tubes (red lines). Measurements of the same samples by IC as an established routine method are shown in blue. Values agree very well, and the average deviation of all values is 6% (IC value = 100%). The IC samples had to be diluted 2–8-fold to obtain the volume required for the injection by the autosampler (100 μL for cations and 800 μL for anions), while CE measurements were done with undiluted porewater and immediately after sampling. Dilution of small volumes introduces an additional error and bears the risk of contamination. Moreover, it is increasingly difficult to retrieve the relatively large volumes of porewater required by IC with increasing sediment depth as the water content decreases with depth from close to 100% at the surface to 80% at 5 cm and 70% at 15 cm. Collection of larger volumes required extended sampling time and thus increased the risk of Fe(II) oxidation and loss of vertical resolution. In our experiments, it was not feasible to collect enough porewater for IC analyses below a 5.5 cm core depth. In addition, the detection limits of IC for Fe(II) and DIP were insufficient, and analysis with other methods could not be accomplished due to the small sample volume.

Subsurface peaks of NH_4^+, Mn(II) and Fe(II) in the top sediment layer originate from the most recent settling of a spring algae bloom. The high amount of organic matter was subject to immediate mineralization consuming easily available electron acceptors such as oxygen O_2, NO_3^- and SO_4^{2-} and subsequently even Mn(IV)- and Fe(III)-oxy-hydroxides releasing NH_4^+, Mn(II) and Fe(II).

The simultaneous fluctuations of the profiles (Fig. 3) may be caused by the laminated structure of the sediment. The varves consist of alternating layers of biogenically precipitated calcite of 1–2 mm magnitude deposited after the first algae bloom in spring, and black layers of organic rich material of similar thickness deposited during summer and autumn. The average sedimentation rate of Lake Baldegg is 3.4 mm *per annum*.[31] The diameter of the MicroRhizon sampler tube is only 1 mm and thus in the same range as the sediment laminae. Incidental insertion of the sampler in a calcite-rich sediment layer may thus result in slightly different concentrations of porewater constituents than in an organic rich layer.

While the sampling and analysis of Mn(II) is usually straightforward, the collection of Fe(II) from porewater is

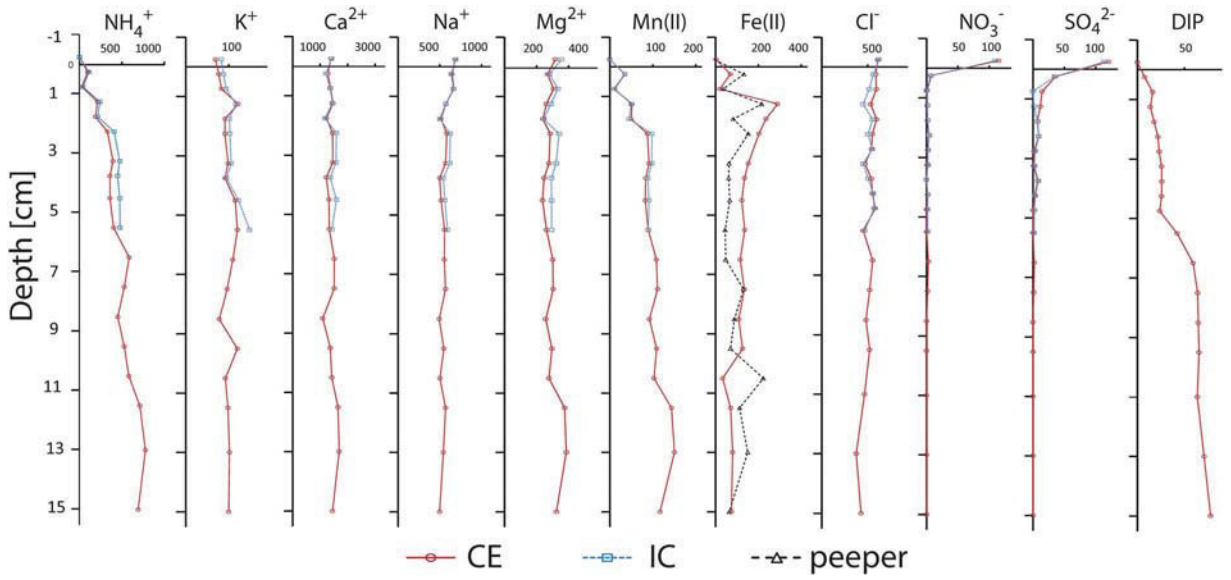

Fig. 3 Porewater concentration (μmol L^{-1}) profiles from sediment cores of Lake Baldegg collected in April (cations) and June (anions) 2012. Blue dots are IC measurements of the same samples (sufficient volume was available until 5.5 cm) and archived Fe^{2+} samples were collected directly from the bottom of the lake with a "peeper" and measured with AAS (dashed line; B. Wehrli, unpublished results).

difficult due to its immediate abiotic oxidation when in contact with O_2. Its sensitivity towards O_2 usually requires handling of sediment cores in a N_2 atmosphere and therefore in glove boxes. Porewater collection by diffusion plates (peepers) is subject to unknown bias due to the contact of the facility with oxic water during retrieval.[32] Here, the porewater collection with MicroRhizon samplers from closed sediment cores reduces the contamination with O_2 to a minimum, and injection into the CE capillary is accomplished in less than 20 seconds allowing analysis of Fe(II) within the set of cations (Fig. 2) without sample splitting, acidification or dilution. Data obtained in previous studies[17] showed no significant difference between sampling in a glove box and sampling in ambient air with the MicroRhizons.

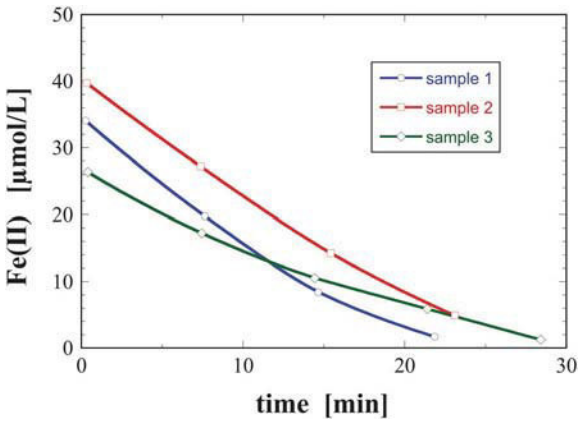

Fig. 4 Kinetic experiment depicting the loss of Fe(II) with time between sampling and injection of the sediment porewater into the capillary (buffer pH 4.1). The initial oxidation of Fe(II) follows a zero-order kinetic.

Fig. 4 shows a simple kinetic experiment to investigate the potential loss of Fe(II) in the vial after sampling. Three porewater samples were injected and measured at different time intervals after retrieval from the sediment core. The first injection was made immediately after sampling (<20 seconds). Three to four further measurements of the same samples, stored in the vials without shaking, were carried out at even time intervals to estimate the oxidation rate. In spite of the oxidation of Fe(II) being a second order process (depending on the concentration of the Fe^{2+} species and O_2 (ref. 33)) we observed an initial linear decrease of Fe(II) concentrations (Fig. 4), originating from the diffusion of O_2 from the atmosphere to the sample solution.

The entire Fe(II) content was found to be oxidized after less than 30 minutes. Linear extrapolation of the initial consumption rate to time zero shows that the loss of Fe(II) in the time between sampling and measurement (20 seconds) is negligible and within the range of the standard deviation of ~5%. These results demonstrate that our method is fast enough to analyze Fe(II) with a minimum error. It emphasizes the high practical value of the proposed method for fast, simple and inexpensive porewater analysis with a minimum bias.

4 Conclusion

The new method, consisting of a combination of MicroRhizons for sampling and a portable capillary electrophoresis instrument for analysis, was successfully applied in the investigation of sediment porewaters of Lake Baldegg. We achieved a full separation of the major inorganic anions and cations, inclusive of manganese(II) and ferrous iron, in less than 15 minutes. MicroRhizon tubes allowed safe handling and sampling of sediment cores in high spatial resolution with minimal disturbance of the sediment structure and zero-oxygen conditions

during sampling without laborious precautions. Due to the fact that porewater from sediment cores can be analyzed accurately without sample splitting, acidification or dilution, the presented method probably is the most rapid technique for sediment porewater analysis without losing accuracy. The accuracy was verified by analyses using ion chromatography. The lightweight and low-cost CE analyzer runs on mains power as well as battery power and is thus well suited for environmental on-site measurements.

Sediment porewater concentration gradients allow the estimation of fluxes of oxidizing agents involved in the mineralization of organic matter in the sediment (NO_3^-, SO_4^{2-}, Mn(II) and Fe(II)), and released nutrients (NH_4^+, DIP). The possibility of accomplishing fast and unsophisticated sediment porewater sampling and reliable measurements of these ions is essential for the monitoring of seasonal variations and for extended investigations of the mineralization of organic matter at different depths of lakes, from littoral to profundal zones,[34] and to complement monitoring of the water column. To date, only a few of such measurements have been carried out due to the great effort that porewater sampling and measurements require. The combination of the methods presented here will significantly facilitate such projects in the future.

Acknowledgements

This work was supported by the Swiss National Science Foundation (Grant no. 200021-137715). The authors would like to thank Pavel Kubáň for his support with the system installation, Ruth Stierli for the IC measurements, Peter Gäumann for the construction of the CE instrument, and Lawrence Och and Christoph Mayr for helpful discussions.

References

1 S. E. Bufflap and H. E. Allen, *Water Res.*, 1995, **29**, 165–177.
2 J. Seeberg-Elverfeldt, M. Schlüter, T. Feseker and M. Kölling, *Limnol. Oceanogr.: Methods*, 2005, **3**, 361–371.
3 S. Emerson, V. Grundmanis and D. Graham, *Earth Planet. Sci. Lett.*, 1980, **43**, 57–80.
4 N. J. Lusczynski, *Filter-press method for extracting water samples for chloride analysis*, United States Geological Survey, 1961, vol. 1544-A, http://pubs.usgs.gov/wsp/1613f/report.pdf.
5 B. J. Presley, R. R. Brooks and I. R. Kaplan, *J. Mar. Res.*, 1967, **25**, 355–357.
6 W. S. Reeburgh, *Limnol. Oceanogr.*, 1967, **12**, 163–165.
7 M. Bender, W. Martin, J. Hess, F. Sayles, L. Ball and C. Lambert, *Limnol. Oceanogr.*, 1987, **32**(6), 1214–1225.
8 R. A. Jahnke, *Limnol. Oceanogr.*, 1988, **33**(3), 483–487.
9 R. H. Hesslein, *Limnol. Oceanogr.*, 1976, **21**(6), 912–914.
10 J. Lewandowski, K. Rüter and M. Hupfer, *Environ. Sci. Technol.*, 2002, **36**(9), 2039–2047.
11 H. Brandl and K. W. Hanselmann, *Aquat. Sci.*, 1991, **53/1**, 1015–1621.
12 M. Krom, P. Davison, H. Zhang and W. Davison, *Limnol. Oceanogr.*, 1994, **39**(8), 1967–1972.
13 N. P. Revsbech and B. B. Jørgensen, *Adv. Microb. Ecol.*, 1986, **9**, 293–352.
14 D. De Beer and J.-P. R. Sweerts, *Anal. Chim. Acta*, 1988, **219**, 351–356.
15 B. Müller, M. Märki, C. Dinkel, R. Stierli, and B. Wehrli, in *Environmental Electrochemistry: Analyses of Trace Element Biogeochemistry*, ed. M. Taillefert and T. F. Rozan, American Chemical Society Symposium Series 811, Washington DC, 2002, pp. 126–143.
16 J. Seeberg-Elverfeldt, M. Schlüter, M. Kölling and T. Feseker, Rhizon – an excellent pore water sampler for low maintenance collection and filtration of small volume samples, in EGU General Assembly, 25–29 Apr., Vienna, Austria, 2005.
17 L. Shotbolt, *J. Paleolimnol.*, 2010, **44**(2), 695–700.
18 J. Song, Y. Luo, Q. Zhao and P. Christie, *Chemosphere*, 2003, **50**, 711–715.
19 B. P. Knight, A. M. Chaudri, S. P. McGrath and K. E. Giller, *Environ. Pollut.*, 1998, **99**(3), 293–298.
20 A. Spangenberg, G. Cecchini and N. Lamersdorf, *Plant Soil*, 1997, **196**(1), 59–70.
21 T. Tiensing, S. Preston, N. Strachan and G. I. Paton, *J. Environ. Monit.*, 2001, **3**, 91–96.
22 J. Parr, M. Bollinger, O. Callaway, and K. Carlberg, in *Principles of Environmental Sampling*, The American Chemical Society, 2nd edn, 1996.
23 Y. Xu, W. Wang and S. F. Y. Li, *Electrophoresis*, 2007, **28**, 1530–1539.
24 J. P. Hutchinson, C. Johns, M. C. Breadmore, E. F. Hilder, R. M. Guijt, C. Lennard, G. Dicinoski and P. R. Haddad, *Electrophoresis*, 2008, **29**, 4593–4602.
25 M. Ryvolová, J. Preisler, D. Brabazon and M. Macka, *Anal. Chem.*, 2010, **29**, 339–353.
26 P. Kubáň, H. T. A. Nguyen, M. Macka, P. R. Haddad and P. C. Hauser, *Electroanalysis*, 2007, **19**(19–20), 2059–2065.
27 P. Kubáň and P. C. Hauser, *Electrophoresis*, 2009, **30**, 176–188.
28 T. Mai, S. Schmid, B. Müller and P. Hauser, *Anal. Chim. Acta*, 2010, **665**, 1–6.
29 P. Kubáň, M. Reinhardt, B. Müller and P. C. Hauser, *J. Environ. Monit.*, 2004, **6**, 169–174.
30 B. Wehrli, A. Lotter, T. Schaller and M. Sturm, *Aquat. Sci.*, 1997, **59**(4), 285–294.
31 A. Lotter, M. Sturm, J. Teranes and B. Wehrli, *Aquat. Sci.*, 1997, **59**(4), 304–325.
32 N. R. Urban, C. Dinkel and B. Wehrli, *Aquat. Sci.*, 1997, **59**, 1–25.
33 W. Stumm and J. Morgan, *Aquatic Chemistry*, John Wiley and Sons, New York, 1996.
34 B. Müller, L. Bryant, A. Matzinger and A. Wüest, *Environ. Sci. Technol.*, 2012, **46**, 9964–9971.

2.2 Early diagenetic processes generate iron and manganese oxide layers in the sediments of Lake Baikal, Siberia

Environ Sci Process Impacts. 2014 Apr;16(4):879-89. doi: 10.1039/c3em00676j.

Volume 16 | Number 4 | April 2014 | Pages 615–944

Environmental Science
Processes & Impacts

rsc.li/process-impacts

ISSN 2050-7887

ROYAL SOCIETY OF CHEMISTRY

PAPER
Beat Müller *et al.*
Early diagenetic processes generate iron and manganese oxide layers in the sediments of Lake Baikal, Siberia

Environmental Science
Processes & Impacts

PAPER

Cite this: *Environ. Sci.: Processes Impacts*, 2014, **16**, 879

Early diagenetic processes generate iron and manganese oxide layers in the sediments of Lake Baikal, Siberia

Natascha T. Torres,[ab] Lawrence M. Och,[a] Peter C. Hauser,[b] Gerhard Furrer,[c] Helmut Brandl,[d] Elena Vologina,[e] Michael Sturm,[f] Helmut Bürgmann[a] and Beat Müller*[a]

Received 10th December 2013
Accepted 30th January 2014

DOI: 10.1039/c3em00676j

rsc.li/process-impacts

Distinct layers of iron(III) and manganese(IV) (Fe/Mn) oxides are found buried within the reducing part of the sediments in Lake Baikal and cause considerable complexity and steep vertical gradients with respect to the redox sequence. For the on-site investigation of the responsible biogeochemical processes, we applied filter tube samplers for the extraction of sediment porewater combined with a portable capillary electrophoresis instrument for the analyses of inorganic cations and anions. On the basis of the new results, the sequence of diagenetic processes leading to the formation, transformation, and dissolution of the Fe/Mn layers was investigated. With two exemplary cores we demonstrate that the dissolution of particulate Fe and Mn is coupled to the anaerobic oxidation of CH_4 (AOM) either *via* the reduction of sulphate (SO_4^{2-}) and the subsequent generation of Fe(II) by S(−II) oxidation, or directly coupled to Fe reduction. Dissolved Fe(II) diffuses upwards to reduce particulate Mn(IV) thus forming a sharp mineral boundary. An alternative dissolution pathway is indicated by the occurrence of anaerobic nitrification of NH_4^+ observed at locations with Mn(IV). Furthermore, the reasons and consequences of the non-steady-state sediment pattern and the resulting redox discontinuities are discussed and a suggestion for the burial of active Fe/Mn layers is presented.

Environmental impact

Early diagenetic processes in sediments lead to the formation of distinct accumulations of particulate Fe and Mn at the oxic–anoxic interface. Using on-site porewater measurements of Mn(II), Fe(II), NH_4^+, NO_3^-, and SO_4^{2-} and later analysis of the solid phase for Mn and Fe, we hypothesize that these layers accumulated with the growing sediment but at some point were halted and subsequently buried in the sediment. This unique pattern of incidental burials of oxidized layers in the reducing (methanogenic) sediment introduces considerable heterogeneities and leads to very unusual diagenetic redox reactions. This manuscript provides the first concise description of the entire diagenetic sequence of processes induced by the Fe/Mn layers from (i) the formation of the Fe/Mn accumulations at the oxic–anoxic interface, (ii) the reductive dissolution of buried layers, and (iii) mechanisms leading to the burial of Fe/Mn layers.

1 Introduction

Lake Baikal is probably the oldest (30–40 Ma[1]), and, with a maximum depth of 1637 m, the deepest and the most voluminous lake in the world. The lake is situated on an active continental rift in southeastern Siberia, the Baikal Rift Zone, separating the Siberian craton in the northwest from the Mongolian–Transbaikalian belt in the southeast *e.g.* ref. 1. The proceeding deepening and the high age of the lake are ultimately the reasons for sedimentary deposits of over 7 km depth, which provide an invaluable archive of geological information often used to reconstruct long-term environmental changes, such as paleoclimate.[2–4] The oligotrophic character of the lake[5] and its pervasively oxygenated water column lead to unusually deep O_2 penetration into the sediment of up to 20 cm.[6]

A special feature of Lake Baikal sediments is the up to 3 cm thick layers of Fe and Mn oxides buried within the reducing part of the sediments and deposited on the deeper plains of all three sub-basins of the lake.[3,7] The origin and the dynamics of the Fe/Mn layers have been hypothesized to be caused by past climate changes[3,8] or tectonic rift events and the ensuing redistribution of Fe and Mn.[9] The Fe/Mn layers cause considerable vertical

[a]*Eawag, Swiss Federal Institute of Aquatic Science and Technology, CH-6047 Kastanienbaum, Switzerland. E-mail: beat.mueller@eawag.ch*
[b]*Department of Chemistry, University of Basel, CH-4056 Basel, Switzerland*
[c]*Institute of Biogeochemistry and Pollution Dynamics, ETH Zurich, CH-8092 Zürich, Switzerland*
[d]*Institute of Evolutionary Biology and Environmental Studies, University of Zürich, CH-8057 Zurich, Switzerland*
[e]*Institute of Earth's Crust, Siberian Branch of RAS, Irkutsk, 664033, Russia*
[f]*Eawag, Swiss Federal Institute of Aquatic Science and Technology, CH-8600 Dübendorf, Switzerland*

discontinuities in the redox sequence commonly observed in sediments[10] and are associated with the diagenetic redistribution of elements such as P, Ca, Sr, As, Sb, and some trace metals.[11] While suggestions for the processes of formation and transformation of Fe/Mn layers at the oxic–anoxic interface were brought forward by Müller *et al.*[11] and Och *et al.*,[12] the ultimate cause for occasional burial is still not clarified. Although some mechanisms have been proposed, such as changes in either the mass accumulation rate of organic carbon, sedimentation rate, porosity, or O_2 supply to the sediment, no conclusive evidence has yet been found.

Och *et al.*[12] hypothesized a cycle characterized by the dynamic growth of Fe and Mn oxide layers right underneath the depth of maximum O_2 penetration, an increasingly slowed down reductive dissolution followed by the burial of the Fe/Mn oxide accumulation and the subsequent initiation of a new dynamic Fe/Mn layer above. Ultimately, the dissolution of the buried Fe/Mn oxide layer is controlled by the anaerobic oxidation of CH_4 (AOM) by SO_4^{2-} and/or Fe oxides in the deeper sediment, and the formation of the upper dynamic Fe/Mn oxide layer by the diffusive flux of O_2 from the water column into the sediment.

Until now, investigating the complex redox chemistry of the Lake Baikal sediments has been limited by the laborious porewater sampling, sampling artefacts such as contamination or the oxidation of dissolved Fe(II), small sample volumes and low concentrations restricting the number of analyses, as well as conservation and transport of the samples. Recently developed portable equipment,[13–15] consisting of MicroRhizon tubes and a portable capillary electrophoresis (CE) instrument,[13,16] allowed determination of *in situ* porewater data with high spatial resolution. Based on these high-quality data, we

- present the processes leading to the formation and transformation of the Fe/Mn layers on the basis of sediments and porewater analyses,
- discuss the reasons and consequences of the non-steady-state situation in the diagenetic process and the discontinuous redox sequence within the Lake Baikal sediments, and
- suggest possible causes for the burial of dynamically accumulating surface Fe/Mn layers into deeper sediments.

2 Materials and methods

2.1 Sampling site and sediment coring

Sediment cores were collected in March 2013 from two sites in the south basin of Lake Baikal (geographic positions: N 51°46′04.2″, E 104°24′33.8″ and N 51°41′33.8″, E 104°18′00.1″) (Fig. 1). The locations were accessed on the ice by a truck equipped with a winch for coring. Ice holes with a diameter of approximately 20 cm were drilled with an engine-driven wimble through the 90 cm thick ice layer to get access to the sediments at 1360 m depth, 14.4 km from the shore (core Baik13-4D, internal codes 'site A' or 'core A') and 3.8 km from the shore (core Baik13-6B, internal codes 'site B' or 'core B'). The following investigations were carried out:

1st core: porewater analysis & solid phase concentration measurements (site A, site B).

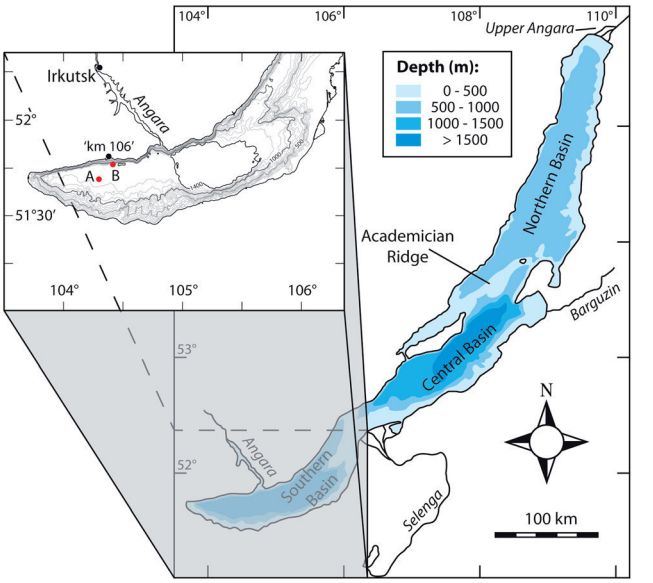

Fig. 1 Map of Lake Baikal and a zoom into the Southern Basin relief. The coring sites A and B are indicated by red dots. Base camp (Neutrino station) was at the shore of the lake near the station 'km 106' of the Circum-Baikal Railway.

2nd core: methane analyses (site A, site B).

3rd core: lithology & magnetic susceptibility, photograph (site A, site B).

4th core: XRF & microbial analyses (site A).

Cores were collected using a UWITEC gravity corer (UWITEC, Mondsee, Austria) with PVC tubes of 6.3 cm diameter and 60 cm length. Tubes for porewater sampling had holes of 0.15 cm diameter drilled staggered with a vertical resolution of 0.25 cm, while tubes for methane samples had holes of 1 cm diameter staggered with a vertical resolution of 1 cm. Modified liners were sealed with tape before coring that was cut open for sampling after retrieval. After the porewater sampling, both cores A and B were extruded in slices of 0.5 cm thickness for the uppermost 15 cm of the sediment and 1 cm thickness for the remaining lower part and transported to Switzerland for sediment analyses. One undisturbed core (only from site A) was transported to Switzerland for the microbial and XRF analyses, and one undisturbed core of each site was transported to the Russian Institute of Earth's Crust for detailed lithological analyses and measurement of the magnetic susceptibility.

Samples for CH_4 analyses were collected immediately after core retrieval. To prevent freezing (air temperature −20 °C) all the other collected sediment cores were immediately brought to the base camp to the improvised laboratories, which were heated to ~15 °C. Electricity was available from the close-by Circum-Baikal Railway line (kilometer 106).

2.2 Porewater sampling and analyses

Equipment for on-site porewater analyses, methane sampling, and sediment extrusion was packed in two boxes and carried on the plane as cabin luggage. We used two portable CE instruments for simultaneous on-site determination of cations and

anions.[13,15] All solutions used for the sediment porewater analyses were prepared and ultrasonicated for 30 minutes at Eawag (Switzerland). Chemicals were of p.a. grade (Sigma-Aldrich, Steinheim, Germany or Fluka, Buchs, Switzerland) and only used with high purity deionized water (Purelab Ultra, ELGA LabWater, UK). The stock solutions of cations were prepared from the corresponding chloride salts. The stock solutions of anions were prepared from the corresponding sodium or potassium salts. Iron(II) standard solutions were prepared in 10^{-4} M HCl (Suprapur©, Merck, Darmstadt, Germany).

The whole equipment for the extraction and analyses of the porewater was set-up at the Neutrino station on the shore of Lake Baikal in the improvised laboratories on two simple working desks and connected to the local power supply. Porewater samples were retrieved from the cores immediately after arrival from the sampling site with MicroRhizon filter tube samplers of 2 cm length, 1–1.1 mm diameter and 0.15–0.20 μm pore size (Rhizosphere Research Products, Wageningen, Netherlands). They were connected to a 1 ml syringe and inserted horizontally into the staggered holes of the corer to draw 10 to 30 μl of porewater from the sediment. The samples were transferred to 1 ml PE centrifuge tubes and immediately injected into the portable CE instrument for measurement. Blanks (high purity deionized water collected with MicroRhizon samplers) and certified multi-element ion chromatography standard solutions (Fluka, Buchs, Switzerland) were intermittently measured to ensure a high data quality. The relative standard deviations of triplicate sample measurements were <5% for each ion.

For the data acquisition TraceDec® C^4D detectors (Innovative Sensor Technologies GmbH, Strasshof, Austria) were used and the signals were recorded with the TraceMon software application. The peaks were analyzed using the Chart Software (version 5.5.8) from eDAQ (Denistone East NSW 2112, Australia). Fused silica capillaries (50 μm i.d., 360 μm o.d., 55 cm length) (BGB Analytik AG, Böckten, Switzerland) were used for separation. The capillaries were preconditioned with 1 M NaOH for 5 minutes, rinsed with high purity deionized water for 5 minutes, preconditioned with 1 M HCl for 5 minutes, rinsed again with high purity deionized water for 5 minutes, and finally equilibrated with the electrolyte solution for at least 30 minutes. A voltage of 15 kV was applied to the buffer vials. The sample was injected hydrodynamically by elevating the capillary end immersed in the sample vial for an injection time of 20 seconds at 15 cm height for anions and 8 cm for cations. The sampling and measurement of one sampling point was accomplished in maximum 15 minutes. Eight cations (NH_4^+, K^+, Ca^{2+}, Na^+, Mg^{2+}, Mn^{2+}, Fe^{2+}, and Li^+) and six anions (Cl^-, NO_3^-, SO_4^{2-}, NO_2^-, F^-, and PO_4^{3-}) were fully detected in less than ten minutes from an undiluted and immediately injected sample. Data evaluation and preliminary interpretation were done on the same day and therefore a maximum of flexibility in decision-making for further coring was provided on-site.

2.3 Additional analyses and procedures

Methane. Samples for CH_4 measurements were taken immediately after coring on the ice. Sediment sub-cores of 2 cm^3 volume were collected by insertion of a plastic syringe that was cut open at the tip through the pre-drilled holes. The tape covering the holes was cut open with a knife. The sub-samples were subsequently transferred into a serum flask containing 2 ml of 10 M NaOH and sealed with a butyl septum stopper. CH_4 was determined by headspace analyses with an Agilent gas chromatograph (Agilent Technologies AG, Basel, Switzerland) equipped with a Supelco Carboxene®-1010 column (Sigma-Aldrich, Steinheim, Germany), at the Eawag laboratory in Switzerland.

Water content and porosity. The water content was determined by weight difference before and after freeze-drying. The porosity (ϕ) was estimated using an empirical relationship comprising TOC and water content.[5]

Solid phase analyses. The extruded sediment samples were freeze-dried and ground in an agate mortar at Eawag. Fe and Mn were determined after oxidative digestion (4 ml HNO_3 conc. and 1 ml H_2O_2 in a microwave oven for 30 minutes) with an ICP-MS (Agilent 7500 series, Agilent Technologies AG, Basel, Switzerland). Total carbon (TC) and total sulphur (TS) were determined by thermic combustion using an element analyzer, Euro EA 3000 (HEKAtech, Wegberg, Germany). Total inorganic carbon (TIC) was determined using a coulometer (CM5015, UIC, Joliet, IL 60436, USA) and total organic carbon (TOC) by thermic combustion using an element analyzer, Euro 3000 (HEKAtech, Wegberg, Germany).

Lithology and magnetic susceptibility. The cores were cut longitudinally, photographed and analyzed for detailed lithology, using smear slides and measurements of magnetic susceptibility. The magnetic susceptibility was determined using a Bartington GT-2 surface probe (Bartington Instruments, Witney, Oxford, OX28 4GE, England) at intervals of 1 cm at cores that were cut open.[17,18]

XRF core scanning. A whole core of 35 cm length from site A was transported to Eawag, split in half along the length and opened. One half was used for a highly resolved and non-destructive determination of the Fe and Mn composition longitudinally using an Avaatech X-Ray Fluorescence (XRF) core scanner (Avaatech XRF, 1812 PS Alkmaar, Netherlands). The core was analyzed at 10 kV using steps of 2 and 5 mm, depending on the visually determined complexity of the sediment. The qualitative profile of Fe and Mn was subsequently calibrated according to the values from the ICP-MS analysis.

Microbiology. The other half of the opened core (see XRF core scanning) was sampled for microbial cell counting following Zarda *et al.*[19] Samples were taken from 35 different depths from the 35 cm long core and obtained by sectioning the core in 0.5 cm intervals with sterile metal disks and transferring each section into sterile 15 ml polypropylene tubes. Subsamples of 0.5 g of sediment were fixed overnight in 4% paraformaldehyde in phosphate buffered saline (PBS) at 4 °C. Fixed samples were washed twice with PBS and stored in 1 : 1 ethanol–PBS at −20 °C until analysis. Samples were stained with 4′,6-diamidino-2-phenylindole (DAPI) and analyzed following established protocols.[19] Stained cells were counted on 24 fields from two independently spotted wells per sample using a Zeiss Axioscope 2 epifluorescence microscope (Carl Zeiss AG, Oberkochen, Germany).

Flux calculations. Areal porewater fluxes (J_{sed}) were determined from concentration gradients applying Fick's first law of diffusion *e.g.* ref. 20.

$$J_{sed} = \phi D_{sed} \frac{dC}{dx}$$

$$D_{sed} = \frac{D_0}{\phi F}$$

Molecular diffusion coefficients (D_0) at 4 °C were taken from Li & Gregory.[21] D_{sed} was calculated using the porosity ϕ and the formation factor F as suggested by Maerki *et al.*[22]

$$F = 1.02\phi^{-1.81}$$

3 Results and discussion

3.1 Formation, transformation, and dissolution of Fe/Mn layers

The characteristic pattern of black layers of Mn oxides overlying thin layers of ochre colored Fe oxides in the top few centimeters of the sediment is widespread in Lake Baikal sediments and the occurrence of two or more layers is frequently observed.[7,8,23] Two principal types of layers could be distinguished in cores from sites A and B depicted in Fig. 2 and 3. As demonstrated by Och *et al.*,[12] the uppermost Fe/Mn enriched layer is commonly located right below the O_2 penetration depth, *i.e.* the O_2–Mn(II) redox interface, followed by Fe/Mn layers buried in the deeper, reducing parts of the sediments.

3.1.1 Core description. The data of cores from site A are given in Fig. 2. Five apparent peaks of particulate Mn are clearly distinguishable from the background content of 0.1%. While the uppermost accumulation is minor (Peak # 1), the highest two are found within a short interval between 5.5 and 8 cm depths within the Mn-reducing part of the sediment (Peaks # 2 and # 3) and two additional maxima occur at 13 cm and 18.5 cm (Peaks # 4 and # 5) depths. Accumulations of particulate Fe are observed at the same sediment depths as the Mn peaks, or slightly below (Peaks # 1 and # 2). The background concentration of particulate Fe, predominantly Fe oxides,[12] is about 4%. The porewater Mn(II) concentration increases from below detection limit underneath the uppermost Mn oxide layer, peaks around the maximum particulate Mn accumulations and decreases towards Peak # 4 at around 14 cm depth. Concentrations of dissolved Fe(II) are mostly below the measurable concentration range down to 9 cm depth with an exception at 4.5 cm, where an isolated peak of 7.5 μmol l^{-1} occurs. Below 9 cm, between two Fe oxide peaks, a steep increase is observed, culminating to a maximum of 51 μmol l^{-1} at a depth of 11 cm before steeply decreasing again down to ~15 μmol l^{-1}.

The data of cores from site B are given in Fig. 3. The particulate Mn content in the top layer was high (2.3%) and formed a peak (# 1) of up to 3.5% at 2.25 cm depth. Below 3 cm depth, a sharp decrease to background concentrations of around 0.1% is observed above a second peak (# 2) of 0.82% occurring at 10.25 cm depth. Like in core A, background contents of the particulate Fe were around 4%. Two major peaks were observed, where the first reached 6.3% right underneath the upper particulate Mn peak at 2.75 cm depth (Peak # 1), and the second reached 9.8% at the same depth as the lower particulate Mn peak (# 2). A slight increase in the Fe content occurred at a depth of around 14 cm (Peak # 3).

Porewater Mn(II) is first detected at 1.25 cm sediment depth. The concentration increases sharply to 41 μmol l^{-1} at 2 cm

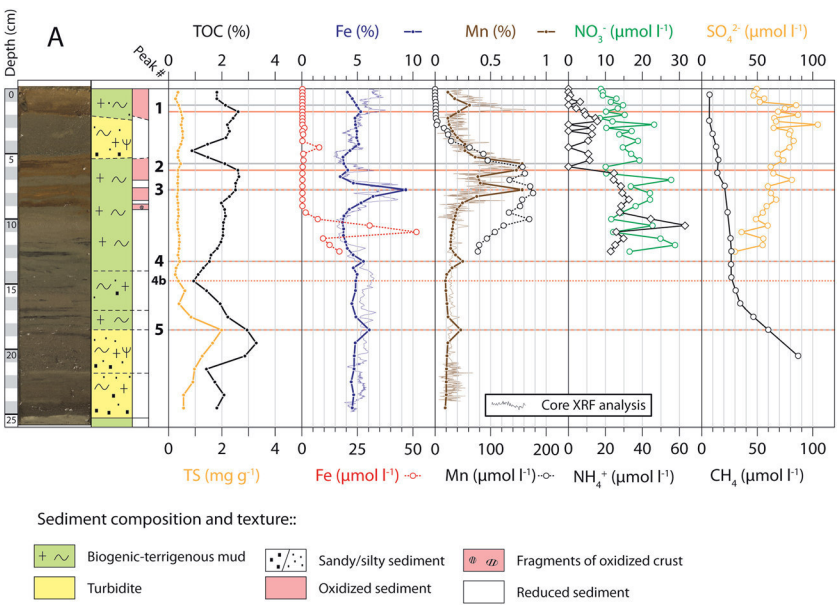

Fig. 2 Core A, its lithology, composition, and the geochemical profiles as discussed in the present study. Fe and Mn oxide enrichments discussed in the text are numbered (#).

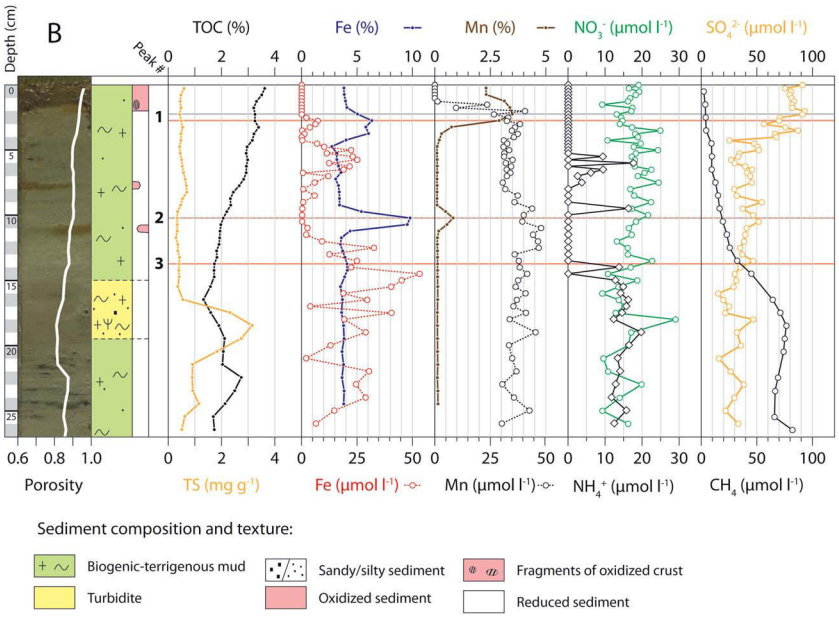

Fig. 3 Core B, its lithology, composition, and the geochemical profiles as discussed in the present study. Fe and Mn oxide enrichments discussed in the text are numbered (#).

depth and remains relatively constant at 30–48 µmol l^{-1} for the remaining part of the analyzed core. Porewater Fe(II) always increased right below the Fe oxide accumulations. The concentration varies around a maximum of 7.2 µmol l^{-1} at ~5.75 cm and a maximum of 53 µmol l^{-1} at ~14.5 cm.

3.1.2 Formation and transformation of the upper Fe/Mn layer. The observation of similar multiple Fe/Mn layers in the uppermost ~50 cm of the sediments is rather exceptional and has so far been described not only from equatorial upwelling systems in the Atlantic and Pacific Oceans *e.g.* ref. 24 and the Centrals Arctic Ocean *e.g.* ref. 25–27, where they have been linked to climate variability, but also in lacustrine and marine environments such as in some settings of the Great Lakes[28,29] and Loch Lomond in Scotland.[30]

The low primary productivity[5] and efficient deep water mixing[31] of Lake Baikal ensure permanently oxygenated bottom water and an exceptionally high O_2 penetration depth.[6] Therefore, all the settling manganese and iron have been trapped within the sediments since the formation of Lake Baikal, and reductive dissolution sets in only several centimeters below the sediment surface. This situation is like that of the Central Arctic Ocean, which has been a low-productivity and well-ventilated setting through most of the quaternary, with deep O_2 penetration depths, and trapping of almost all settling Fe/Mn oxides within the deep basins.[32]

Due to the low sedimentation rates of 0.4–0.8 mm a^{-1} in the south basin[12,33] and the high O_2 penetration depth, Mn(II) and Fe(II) from the reductive dissolution of their respective oxides diffuse upwards from the deeper sediment and are re-oxidized to Mn(IV) and Fe(III) accumulating as soon as porewaters contain appreciable O_2 concentrations again. The upper Fe/Mn accumulation (Peak # 1 in Fig. 2 and 3) is located at the active redox interface where upward diffusing Mn(II) is oxidized. Och *et al.*[12] have shown that O_2 penetrates the sediment surface down to the uppermost Mn oxide layer, which is located at 1 cm in core A and 1.25 cm in core B. In both cores the Fe layer as well as the peak of dissolved Fe(II) are positioned a few millimeters below the Mn layer, indicating that dissolved iron is oxidized in contact with Mn(IV), a fast abiotic reaction.[34,35] Thus, reducing conditions at the lower end of the Fe/Mn layer and oxidizing conditions on top (which is O_2 for Mn(II), and Mn(IV) for Fe(II)) allow for a dynamic adjustment of the solid phase Fe/Mn layer to the upward-moving redox interface of the accumulating sediment.

While the concentration profiles of particulate Fe and Mn as well as porewater Mn(II) of our cores are quite comparable with previous studies of Granina *et al.*[7] and Och *et al.*,[12] the Fe(II) profiles are markedly different, in particular within the upper oxic interval of the cores. Indeed, the presence of dissolved Fe in the uppermost oxic sediment layers as reported by Granina *et al.*[7] (Fig. 5b/d) and Och *et al.*[12] (Fig. 2 and 3) cannot, according to thermodynamic considerations, be Fe(II). Our measurements confirm previous arguments that a significant portion of Fe measured by ICP-MS after filtration through a 0.45 µm membrane and acidification with 5 µl HNO_3 can be attributed to colloidal iron.[36] The CE technique applied for porewater analyses in the present study guarantees the specific detection of dissolved Fe(II) *e.g.* ref. 37. Fig. 2 and 3 show that reduced Fe(II) in cores A and B was detected right below the top Mn layers and, thus, the upper limit of the iron reduction zone can be determined precisely with this analytical approach.

We expect that porewater profiles experience no significant influence from the inter-annual variability of physical parameters in Lake Baikal. First, because sedimentation rates are very low and predominantly originate from autochthonous deposition and second, seasonal convective mixing of the water

column does not reach beneath 300 m depth.[31,38] There are, however, diatom blooms which occur every 3 to 5 years in spring which can influence porewater profiles in shallow sediment depths over short periods of time.[5]

3.1.3 Dissolution of buried Fe/Mn layers. Both cores contain one or more Fe/Mn oxide layers (Peak # 2 in Fig. 2, Peaks # 2 and 3 in Fig. 3) buried in the reducing sediment, *i.e.* below the upper dynamic Fe/Mn oxide layers. Such buried layers have even been found in the Baikal sediment up to 65 000–85 000 years old[3] and, as is apparent from the porewater profiles of Fe(II), Mn(II), phosphate and other compounds[11] dissolve slowly, thereby providing additional Fe and Mn to younger sediment layers. The TOC content in Lake Baikal sediments is rather high throughout the cores (between 1 and 3% in core A and 1–3.6% in core B), suggesting that the organic carbon is, to a certain degree, refractory with a diminished electron donor capacity. This is particularly evident since sedimentation rates are low, notably around 0.4 mm in this area of the lake,[33] meaning that the turbidites below Peak # 5 in core A and Peak # 3 in core B result from 500 and 400 year old events respectively. The highly variable TOC profile in core A likely results from the numerous turbiditic depositions and is not directly correlated with the Fe/Mn oxide enrichments. Nonetheless, substantial CH_4 fluxes from the deeper sediment indicate that organic matter degradation remains an important driving force for early diagenesis but it is likely that CH_4 is the key electron donor in this system. Thus, considering CH_4 as the ultimate electron donor, we will discuss the sequence of redox reactions starting from the bottom of the analyzed cores. In each core, CH_4 is predominantly consumed within short intervals close to the occurrence of buried Fe (and Mn) oxides, *e.g.* at 16.5 cm depth in core A and 13 cm depth in core B. CH_4 can be oxidized not only anaerobically (AOM) by sulphate,[39,40] but potentially also by Fe and Mn oxides[41] and NO_3^-.[42] These methane oxidation processes can thus contribute to the production of reduced species such as S(−II), Fe(II), Mn(II), and NH_4^+.

The Fe(II) released from the deepest layers diffuses to the overlying Mn(IV) layer and is oxidized, thus releasing Mn(II),[35] as can be seen in Fig. 2 (Peak # 2).

The present data do not allow deciding whether CH_4 is oxidized by sulphate or rather by Fe oxides. While there might be a clarifying intersection between the CH_4 and SO_4^{2-} profiles in core A if the downward trend in SO_4^{2-} concentrations is extrapolated linearly, indicating AOM by sulphate, we do not see a significant effect in the SO_4^{2-} profile of core B. If CH_4 was oxidized by SO_4^{2-}, we would postulate a cryptic sulphur cycle, where produced S(−II) is recycled to S^0 in contact with Fe(III) oxides.[43–45] It has been shown, however, that further oxidation of S^0 by Fe(III) is inefficient as opposed to oxidation by Mn(IV).[46–49] Hence, if Fe oxides were directly reduced by CH_4, 8 moles Fe^{2+} must be released for every mole of oxidized CH_4:[41]

$$CH_4 + 8Fe(OH)_3 + 15H^+ \rightarrow HCO_3^- + 8Fe^{2+} + 21H_2O \quad (1)$$

However, if SO_4^{2-} was reduced by CH_4 prior to the reductive dissolution of Fe oxides by the resulting sulphides, only 2 moles of Fe(II) are generated by the oxidation of 1 mole CH_4 according to:

$$CH_4 + SO_4^{2-} \rightarrow HCO_3^- + HS^- + H_2O \quad (2)$$

$$2FeOOH + HS^- + 5H^+ \rightarrow 2Fe^{2+} + S^0 + 4H_2O \quad (3)$$

A constant supply of SO_4^{2-} is indicated around the buried Fe/Mn accumulation in most Lake Baikal surface sediments (due to a cryptic sulphur cycle[12]). Hence, the oxidation of S^0 is likely to involve either Mn(IV) oxides[47] or other microbial pathways, such as through *Thioploca* spp. or through disproportionating bacteria from sulphur intermediates.[49] Considering a pathway involving the oxidation of S^0 by Mn(IV)[47] the resulting reaction can be summarized as:

$$CH_4 + 2FeOOH + 3MnO_2 + 9H^+ \rightarrow HCO_3^- + 2Fe^{2+} + 3Mn^{2+} + 7H_2O \quad (4)$$

As the reaction is faster than the diffusion of CH_4, only small amounts of SO_4^{2-} may be required to keep up the transfer of electrons from CH_4 to Fe(III) and may not cause detectable effects in the SO_4^{2-} concentration profile. In order to test whether the above considerations make sense stoichiometrically, we performed diffusive flux calculations using porewater Mn(II), Fe(II) and CH_4 profiles.

It is more suitable to start with core B as the porewater profiles extend down to greater depth and are more suitable to illustrate our case. There, the upward methane flux towards Peak # 3 in Fig. 3 is ~15 mmol m^{-2} a^{-1}. Assuming that the AOM involving Fe oxides lead to the release of Fe(II) without the formation of solid phases or consumption by MnO_2, we expect an either eightfold (reaction (1)) or a twofold (reaction (4)) higher flux of Fe(II), *i.e.* ~120 mmol m^{-2} a^{-1} Fe(II) or ~30 mmol m^{-2} a^{-1} Fe(II). Although the Fe(II) concentrations were very variable across the core, we can evaluate the flux according to a more schematic profile characterized as a succession of peaks with amplitudes increasing with depth. As a result, the dissolution rate of Fe oxides at Peak # 3 is at least 20 mmol m^{-2} a^{-1}. However, if the interval taken for the calculation of the fluxes is reduced to the immediate vicinity of Peak # 3 (Fig. 3), *i.e.* between 13 and 16 cm depths, the dissolution rate of Fe oxides increases to 50 mmol m^{-2} a^{-1}. Hence, observed Fe oxide dissolution rates are between 20 and 50 mmol m^{-2} a^{-1} and thus support a pathway where AOM proceeds through the reduction of sulphate and only indirectly through the reductive dissolution of Fe oxides. However, although reactive Mn oxides are present close to Peak # 3, the precise pathways leading to the formation of SO_4^{2-} are currently not conclusive.

Similarly in core A the CH_4 flux towards the Fe oxide Peak # 4 and/or 4b in Fig. 2 was >25 mmol m^{-2} a^{-1} and could therefore release a maximum of ~200 mmol m^{-2} a^{-1} Fe(II) (reaction (1)) or ~50 mmol m^{-2} a^{-1} (reaction (4)), respectively. Unfortunately there are not enough porewater data to calculate meaningful Fe oxide dissolution rates but the presence of such small Fe oxide accumulations as in Peaks # 4, 4b and 5 would be highly unlikely if the AOM would directly reduce Fe oxides rather than sulphate. Hence, we suggest that the pattern in core A also points toward the oxidation of CH_4 by sulphate and subsequent formation of elemental S by the reduction of Fe(III).

3.2 Redox discontinuity caused by the Fe/Mn layers

The incidental burials of oxidized layers of Fe and Mn in the methanogenic sediment introduce zones of slowly reacting electron acceptors with a large capacity. Thus, the continuous succession of redox reactions usually observed in sediments allowing for a steady-state situation between provision of organic matter at the sediment surface and a subsequent degradation by the typical cascade of electron acceptors at depth, as sketched *e.g.* by Froelich *et al.*,[10] does not hold for Lake Baikal sediments. The oxidized zones of the slowly reacting Fe/Mn phases embedded in a reducing environment cause complex interactions in the vertical diagenetic profile.

Vertical heterogeneity caused by short-term sedimentary events disrupts steady-state processes and might temporarily stimulate microbial growth.[50–52] The microbial distribution across core A (Fig. 4) reflects the overall heterogenetic character of Lake Baikal sediments.

Interestingly, peaks in the cell counts coincide with peaks of Mn(IV) and in particular Fe(III) enrichments, prompting the conclusion that the biogeochemical cycling of Mn and Fe shaped the microbial communities in the surface sediments of Lake Baikal. Hence, early assumptions can be made regarding the dominant microbial pathways involved in the Fe and Mn cycling: (1) the uppermost 2 cm may harbor Mn oxidizing (aerobic) microbes while the underlying 2 cm are likely to be dominated by Fe oxidizing microbial pathways coupled to organic matter degradation. (2) Although a large cell peak is observed within the layer of maximum Mn enrichment, the highest cell counts correlate better with smaller peaks in the Fe content and therefore might indicate microbial pathways that reductively dissolve Mn oxide by Fe(II). (3) Below 10 cm, the microbial abundance is rather low but increases again at the next buried oxide layer between 23 and 26 cm, possibly reflecting the presence of a microbial community based on methanotrophy. Further studies into the phylogenetic and functional composition on the microbial community would be required to test these hypotheses.

3.2.1 Anaerobic nitrification by Mn oxides. Porewater nitrate was observed throughout all investigated cores in concentrations of 10–20 μmol l^{-1}. These concentrations were higher than in the overlying water (~10 μmol l^{-1}) and could therefore not be caused by diffusion through the sediment–water interface but must originate from anaerobic nitrification in the sediment. Two questions arise in this context: first, what is the oxidant that causes nitrification in the anaerobic sediment, and second, why does NO_3^- persist in the porewater and is it not denitrified by the available reductants?

The NH_4^+ porewater profiles (Fig. 2 and 3) are unsteady in both sediment cores. In homogeneous sediments, a smooth increase in the concentration of NH_4^+ with depth is usually observed, as it is the degradation product of amino acids in an anoxic environment. However, NH_4^+ can be re-assimilated into biomass or sorb onto clay minerals and/or re-oxidized to nitrite or nitrate during nitrification or anaerobic ammonium oxidation *e.g.* ref. 53–57.

In core A (see Fig. 2), NH_4^+ is already detected at 0.5 cm depth, followed by a two-step increase, initially to 10–15 μmol l^{-1} at 1 cm and, after a few incidental excursions back to zero, to ~30 μmol l^{-1} at 6.5 cm. Both steps are delimited by Fe/Mn oxide layers (Peaks # 1 and 2). A single NH_4^+ peak of up to 64 μmol l^{-1} occurs between Peaks # 3 and 4.

In core B (see Fig. 3), NH_4^+ is first detected at 5.5 cm (between Peaks # 1 and 2) before concentrations increase to 18 μmol l^{-1} with zones devoid of NH_4^+ between Peaks # 2 and 3. Steady concentrations of ~15 μmol l^{-1} prevail below 14 cm depth underneath Peak # 3.

Nitrate and ammonium anomalies were found in several other studies and sometimes explained as sampling artefacts due to cell bursting during centrifugation, stress reactions of the sediment fauna during decompression, and warming of the

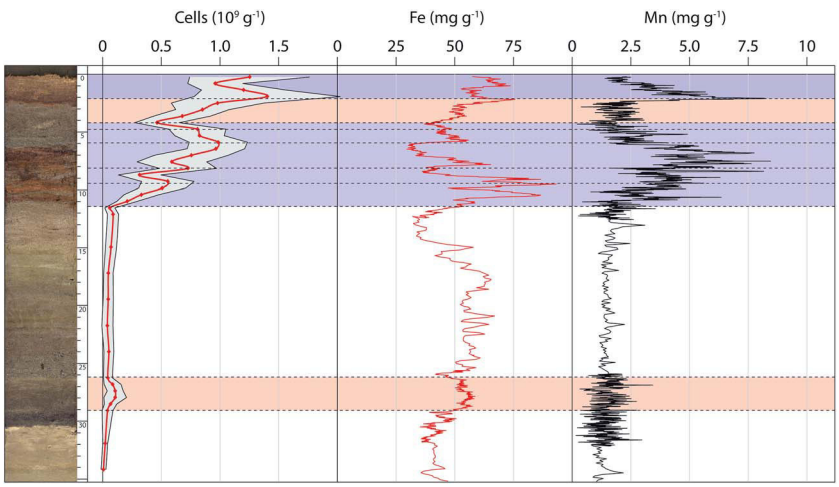

Fig. 4 Depth profile of DAPI-stained cells in the sediment (with standard deviation in grey). The core was taken close to the location of core A. Peaks at 2, 6, 9.5 and 28 cm depth confirm the heterogeneity of the sediment. The peaks coincide clearly with the visible Mn oxide (blackish) and Fe oxide (reddish) layers from the photograph as well as with the XRF scan reflecting Mn and Fe oxide levels. The top peak at 2 cm corresponds to the current oxic–anoxic interface.

sediment core *e.g.* ref. 58 and 59. We also found discontinuous NH_4^+ porewater profiles and the occurrence of NO_3^- in anoxic sediment strata in data from previous field trips to Lake Baikal throughout all porewater measurements using various methods for sampling as well as for analyses (B. Müller, unpublished data). Furthermore, we observed a close correlation between the vertical concentration patterns of NO_3^- and SO_4^{2-} but not with Cl^- (data not shown). Hence, we exclude a bias in the analytical determination of anions by CE. So far, it was unclear whether the exceptional NH_4^+ and NO_3^- concentration profiles represented the true situation or were caused by unknown bias. The results of the on-site measurements in this study, designed to avoid such sampling artefacts, confirmed the previous findings. Due to the irregular occurrence of buried oxidized Fe/Mn layers in the Baikal sediments, the redox sequence is discontinuous, and we do not have a successively increasing reductive intensity with depth. The intermittently distributed oxides of Mn(IV) (and potentially Fe(III)) can act as oxidants for microbially mediated nitrification, which was observed by Luther *et al.*,[60] Aller *et al.*,[61] as well as Anschutz *et al.*,[62] and investigated by Hulth *et al.*[55] and Bartlett *et al.*[53] Anomalies of N species in marine sediments were also observed by several other authors[50,58,63] and more recently also in a lacustrine system.[64] The direct oxidation to N_2 or the oxidation to NO_3^-/NO_2^- and subsequent denitrification are possible. The following equation for anaerobic nitrification was proposed by Hulth *et al.*:[55]

$$4MnO_2 + NH_4^+ + 6H^+ \rightarrow 4Mn^{2+} + NO_3^- + 5H_2O \quad (5)$$

However, there have been difficulties in obtaining conclusive evidence for the anaerobic oxidation of ammonium by Mn oxides.[65,66] Bartlett *et al.*[53] put forward that sediment perturbations might be a prerequisite for the expression of anaerobic nitrification (reaction (5)), be it physical or chemical. The otherwise unusual presence of large amounts of Mn oxides buried in Lake Baikal sediments is likely to represent such a case. Similarly, anaerobic nitrification might occur in the presence of Fe(III)oxides. However, Anschutz *et al.*[50] estimated that this pathway was feasible only when Fe(II) concentrations were low and pH relatively high. Hence, the nitrification of NH_4^+ by Fe oxides was considered less likely than by Mn oxides. A close coupling of reaction (5) with the sulphur cycle is suggested, as the profiles of NO_3^- and SO_4^{2-} often covary (see Fig. 2 and 3), which could be explained by the biogenic oxidation of labile sulphides:[46]

$$4\ MnO_2 + 8H^+ + FeS(s) \rightarrow 4Mn^{2+} + SO_4^{2-} + Fe^{2+} + 4H_2O \quad (6)$$

The simultaneous oxidation of labile S(−II) (and possibly S(0)) and NH_4^+ with reactive MnO_2 particulate surfaces could explain the correlated pattern of NO_3^- and SO_4^{2-} porewater concentrations. However, the unusually high NO_3^- and SO_4^{2-} concentrations reaching deeply into the sediments deserve further considerations and we outline possible processes in the following section.

3.2.2 Nitrate and sulphate anomalies. While the profiles of most species adequately reflect the dominant early diagenetic processes in the surface sediments of Lake Baikal, the detection of NO_3^- and SO_4^{2-} in the methanogenic sediment zones of both cores represent the most unusual result encountered in the present study.

In core A (Fig. 2), NO_3^- concentrations slightly increase with depth and exhibit considerable variations, from 8 μmol l^{-1} at the sediment water interface to 29 μmol l^{-1} at depth. SO_4^{2-} first reaches concentrations of up to 104 μmol l^{-1} at 2.75 cm depth, which is even higher than in the overlying water (49 μmol l^{-1}) and then slowly decreases down to 30 μmol l^{-1}.

NO_3^- concentrations in core B (Fig. 3) remain within the same range as in core A with an average of 17 μmol l^{-1} (16 μmol l^{-1} in core A), a minimum of 9 and a maximum of 29 μmol l^{-1}. The SO_4^{2-} concentrations are up to 90 μmol l^{-1} within the uppermost sediment and decrease down to 50 μmol l^{-1} at a depth of about 4.5 cm. The concentrations remain generally above 20 μmol l^{-1} until the end of the core at 26 cm, but exhibit a sharp decrease underneath the upper Fe and Mn oxide accumulation (Peak # 1) before aligning with NO_3^-. In the previous chapter we discussed biogeochemical reactions that explained the occurrence of these oxidized species in a heterogeneous sediment. However, it is more puzzling how these species could be preserved in sediment where potential reductants such as Mn(II), Fe(II), TOC, and CH_4 are abundant. However, similar concentration profiles were previously observed in Lake Baikal sediments[67,68] (Müller, unpublished data) as well as in other lacustrine[64] and marine surface sediments.[50,63,69]

We calculated the thermodynamic equilibrium for the prevailing chemical conditions of the sediment and found that denitrification by Mn(II) can be ruled out, which is in agreement with the estimations of Hulth *et al.*[55] Testing Fe(II) as a possible reductant for NO_3^- (ref. 70) revealed that the sediment was approximately at equilibrium with the prevailing concentrations, pH 6 and a pN_2 of 1 atm. TOC, in spite of the high sediment content, was already ruled out as a significant reductant for the buried Fe/Mn layers and, apparently, did not affect NO_3^- concentrations in the porewater during the observed time scale (sediment depth) either. It seems that the reactivity of the buried TOC, probably due to its long exposure to oxic conditions, is very low and only slow fermentation at greater depth, *i.e.* a longer time scale, eventually leads to the formation of CH_4. Thus, only CH_4 remains as an unambiguous potential reductant for NO_3^-, at least in thermodynamic terms. Until the recent discovery of a microbial consortium[71,72] that actually linked AOM to denitrification[42] there was no experimental evidence of this reaction and the pathway was considered "missing in nature". Apparently, these microorganisms develop with a very slow growth rate only in the total absence of other oxidants. This may be a reason why this oxidation pathway had never been observed in lacustrine or marine sediments before, and in Lake Baikal it would have to occur at lower rates than the production of nitrate. Considering all the above arguments, we can thus explain the formation and the persistence of NO_3^- in the sediment porewater. Explaining the presence of SO_4^{2-}, however, is more challenging.

The possibility of a cryptic sulphur cycle deeper in the sediment has already been mentioned in Section 3.1.3 but,

unlike previous studies on Lake Baikal sediment porewaters,[12] elevated SO_4^{2-} concentrations are not limited to the intervals with large Fe and Mn oxide enrichments and other microbial pathways should also be considered. Several authors reported the presence of vertically migrating facultative chemoautotrophic sulphide-oxidizing bacteria, *Thioploca* spp. in marine[73–75] and lacustrine environments[76–78] and in Lake Baikal.[68,79,80] They are phylogenetically similar to *Beggiatoa* spp. and are able to pump NO_3^- from the bottom water into the sediment. NO_3^- is accumulated intracellularly to concentrations up to four orders of magnitude higher than bottom-water concentrations.[73] Within their sheaths they can vertically glide down over 15 cm and reduce NO_3^- to NH_4^+ and NO_2^-, concomitant with the oxidation of S(−II), which provides perfect conditions for anammox bacteria too.[81] Interestingly, Zemskaya *et al.*[68] found increased SO_4^{2-} (up to 800 μmol l^{-1}) and NO_3^- (20–500 μmol l^{-1}) concentrations in some *Thioploca* habitats in Lake Baikal sediments. Although we did not find any visual evidence of *Thioploca* filaments in our cores, their potential existence cannot currently be excluded. To obtain further information on the presence of *Thioploca* spp. or *Beggiatoa* spp., we plan to extract the DNA from Lake Baikal sediments and analyze the microbial community composition in a next step.

3.3 Burial of the Fe/Mn layers

Vertical profiles of element contents and porewater fluxes in the sediments allow conclusions on the biogeochemical processes controlling the formation and transformation of Fe/Mn layers right below the O_2–Mn(II) redox interface and the gradual dissolution of buried layers in the reducing (methanogenic) sediment. However, the critical incident required to bury a Fe/Mn layer in the sediment cannot, at present, be investigated by measurements. Four scenarios affecting the position of the O_2–Mn(II) redox interface may be anticipated:

- Changes in the mass accumulation rate of organic matter: an increase of the settling organic matter would increase the sediment oxygen consumption and thus O_2 penetration depth.
- Decreasing bottom water O_2 concentration due to restrained water column mixing would decrease O_2 penetration.
- A growing Fe/Mn layer could at some point constrain the diffusion of dissolved compounds.
- The increasing sedimentation rate would enlarge the diffusive pathway and separate the O_2–Mn(II) interface.

The first two processes might result from climatic variations over the last 1000 years *e.g.* ref. 82, but it is difficult to infer that from the geochemical profiles alone. The third process is unlikely as the diffusivity across the Fe/Mn oxide accumulations is only marginally slower considering the range of calculated porosities in the present study. However, the last process could be confirmed from the lithology of core A, which incidentally shows the occurrence of a turbidite layer of 3 cm magnitude about 0.5 cm right above a Fe/Mn layer (Fig. 5).

Sediment slides, however, are not a frequent cause for the detachment of Fe/Mn layers and we have never observed them above buried Fe/Mn oxide enrichments in other sediment cores from Lake Baikal. To date, none of the other processes suggested above could be evidenced with sediment analyses. Currently, we apply a diagenetic computer model to estimate the constraining variables for the formation, detachment and dissolution of Fe/Mn layers (Och *et al.*, in preparation).

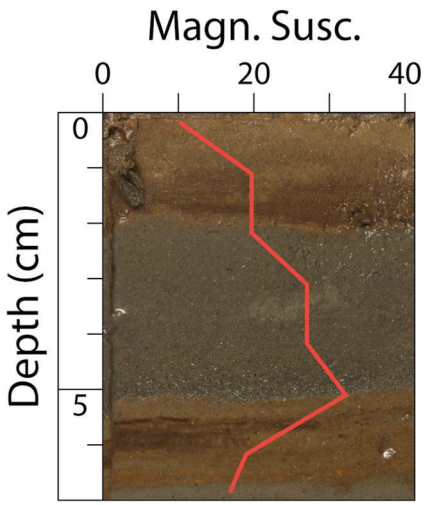

Fig. 5 A turbiditic sediment layer (core A: 2–5 cm depth), clearly visible in the photo and indicated by higher magnetic susceptibility (red line), is overlaying the uppermost buried Fe/Mn layer (below 5 cm).

4 Conclusions

One of the unique features in the Lake Baikal sediments is the redox heterogeneity introduced by the temporally irregular detachment of oxidized layers of Mn and Fe. The occurrence of the resulting sediment structures is rare in such clear patterns, thus allowing the investigation of distinct diagenetic processes and rates. These are mirrored in the porewater samples where the investigation requires advanced analytical equipment to meet the demands of fast sampling, of small volumes, and on-site treatment and analyses.

The application of Rhizon porewater samplers in combination with portable CE instruments with a contact-free detector cell proved to be ideal and reliable for fieldwork even when local working conditions were challenging. Using the resulting porewater data we were able to explain the geochemical reactions leading to the formation and reductive dissolution of Fe/Mn layers and discuss the consequences of diagenetic processes that cause non-steady-state sediment patterns. Concerns about the quality of earlier data from samples of NH_4^+, NO_3^- and SO_4^{2-}, that were hypothesized to change during sampling in Siberia, transportation to and analyses in Switzerland, have been dispelled. Further investigations will be required to fully understand the causes of the presence of SO_4^{2-} in the methanogenic porewater.

Acknowledgements

We are indebted to Professor Nikolay M. Budnev (State University Irkutsk) and Professor Eugene V. Sklyarov (RAS-SB Institute of Earth Crust, Irkutsk) for their support during

fieldwork at Lake Baikal. The authors would like to thank Ursula Brupbacher (ETH Zurich) for the XRF analyses, Serge Robert for the methane analyses, Irène Brunner for TOC and TIC determination, Patrick Kathriner for the water content measurements, David Kistler and Claudio Steger for the metal analyses, Karin Beck for the microbial counts, Beat Kienholz for the core photograph and Michael Schurter for organizing the trip. The project was made possible by the Swiss National Science Foundation (Grant no. 200021-137715).

References

1 V. D. Mats and T. I. Perepelova, *Geosci. Front.*, 2011, **2**, 349–365.
2 D. F. Williams, J. Peck, E. B. Karabanov, A. A. Prokopenko, V. Kravchinsky, J. King and M. I. Kuzmin, *Science*, 1997, **278**, 1114–1117.
3 R. G. Deike, L. Granina, E. Callender and J. J. McGee, *Mar. Geol.*, 1997, **139**, 21–46.
4 T. Sapota, A. Aldahan and I. Al-Aasm, *J. Paleolimnol.*, 2006, **36**, 245–257.
5 B. Müller, M. Maerki, M. Schmid, E. G. Vologina, B. Wehrli, A. Wüest and M. Sturm, *Global Planet. Change*, 2005, **46**, 101–124.
6 P. Martin, L. Granina, K. Martens and B. Goddeeris, *Hydrobiologia*, 1998, **367**, 163–174.
7 L. Granina, B. Müller and B. Wehrli, *Chem. Geol.*, 2004, **205**, 55–72.
8 L. Granina, E. Karabanov and E. Callender, *IPPCCE Newslett.*, 1993, **7**, 32–39.
9 V. D. Mats, O. M. Khlystov, M. De Batist, S. Ceramicola, T. K. Lomonosova and A. Klimansky, *Int. J. Earth Sci.*, 2000, **89**, 229–250.
10 P. N. Froelich, G. P. Klinkhammer, M. L. Bender, N. A. Luedtke, G. R. Heath, D. Cullen, P. Dauphin, D. Hammond, B. Hartman and V. Maynard, *Geochim. Cosmochim. Acta*, 1979, **43**, 1075–1090.
11 B. Müller, L. Granina, T. Schaller, A. Ulrich and B. Wehrli, *Environ. Sci. Technol.*, 2002, **36**, 411–420.
12 L. M. Och, B. Müller, A. Voegelin, A. Ulrich, J. Göttlicher, R. Steiniger, S. Mangold, E. G. Vologina and M. Sturm, *Chem. Geol.*, 2012, **330–331**, 244–259.
13 N. T. Torres, P. C. Hauser, G. Furrer, H. Brandl and B. Müller, *Environ. Sci.: Processes Impacts*, 2013, **15**, 715–720.
14 A. M. Shiller and E. Boyle, *Nature*, 1985, **317**, 49–52.
15 P. Kuban, H. T. A. Nguyen, M. Macka, P. R. Haddad and P. C. Hauser, *Electroanalysis*, 2007, **19**, 2059–2065.
16 R. W. Sterner and J. J. Elser, *Ecological Stoichiometry: The Biology of Elements from Molecules to the Biosphere*, Princeton University Press, 2002.
17 E. G. Vologina, M. Sturm, Y. B. Radziminovich, S. S. Vorob'eva and A. A. Shchetnikov, *Russ. Geol. Geophys.*, 2012, **53**, 1342–1350.
18 N. R. Urban, K. Ernst and S. Bernasconi, *Geochim. Cosmochim. Acta*, 1999, **63**, 837–853.
19 B. Zarda, D. Hahn, A. Chatzinotas, W. Schönhuber, A. Neef, R. I. Amann and J. Zeyer, *Arch. Microbiol.*, 1997, **168**, 185–192.
20 R. A. Berner, *Early diagenesis: a theoretical approach*, Princeton University Press, 1980.
21 Y.-H. Li and S. Gregory, *Geochim. Cosmochim. Acta*, 1974, **38**, 703–714.
22 M. Maerki, B. Wehrli, C. Dinkel and B. Müller, *Geochim. Cosmochim. Acta*, 2004, **68**, 1519–1528.
23 E. G. Vologina, M. Sturm, S. S. Vorob'eva, L. Z. Granina and S. Y. Toshchakov, *Russ. Geol. Geophys.*, 2003, **44**, 407–421.
24 D. J. Burdige, *Earth-Sci. Rev.*, 1993, **35**, 249–284.
25 C. März, A. Stratmann, J. Matthiessen, A. K. Meinhardt, S. Eckert, B. Schnetger, C. Vogt, R. Stein and H. J. Brumsack, *Geochim. Cosmochim. Acta*, 2011, **75**, 7668–7687.
26 L. Löwemark, C. März, M. O'Regan and R. Gyllencreutz, *Quat. Sci. Rev.*, 2014, DOI: 10.1016/j.quascirev.2013.11.018.
27 L. Löwemark, M. O'Regan, T. J. J. Hanebuth and M. Jakobsson, *Palaeogeogr., Palaeoclimatol., Palaeoecol.*, 2012, **365–366**, 192–208.
28 R. Rossmann and E. Callender, *Science*, 1968, **162**, 1123–1124.
29 L. L. Richardson and K. H. Nealson, *J. Great Lakes Res.*, 1989, **15**, 123–132.
30 J. G. Farmer and M. A. Lovell, *Environ. Technol. Lett.*, 1984, **5**, 257–262.
31 M. Schmid, N. M. Budnev, N. G. Granin, M. Sturm, M. Schurter and A. Wüest, *Geophys. Res. Lett.*, 2008, **35**, L09605.
32 R. Macdonald and C. Gobeil, *Aquat. Geochem.*, 2012, **18**, 565–591.
33 U. Morgenstern, R. G. Ditchburn, E. G. Vologina and M. Sturm, *J. Paleolimnol.*, 2013, **50**, 345–352.
34 D. Postma, *Geochim. Cosmochim. Acta*, 1985, **49**, 1023–1033.
35 D. Postma and C. A. J. Appelo, *Geochim. Cosmochim. Acta*, 2000, **64**, 1237–1247.
36 J. Wu, E. Boyle, W. Sunda and L.-S. Wen, *Science*, 2001, **293**, 847–849.
37 J. R. Lead and K. J. Wilkinson, *Environ. Chem.*, 2006, **3**, 159–171.
38 R. F. Weiss, E. C. Carmack Carmack and V. M. Koropalov, *Nature*, 1991, **349**, 665–669.
39 K. Knittel and A. Boetius, *Annu. Rev. Microbiol.*, 2009, **63**, 311–334.
40 C. J. Schubert, F. Vazquez, T. Lösekann-Behrens, K. Knittel, M. Tonolla and A. Boetius, *FEMS Microbiol. Ecol.*, 2011, **76**, 26–38.
41 E. J. Beal, C. H. House and V. J. Orphan, *Science*, 2009, **325**, 184–187.
42 A. A. Raghoebarsing, A. Pol, K. T. van de Pas-Schoonen, A. J. P. Smolders, K. F. Ettwig, W. I. C. Rijpstra, S. Schouten, J. S. S. Damste, H. J. M. Op den Camp, M. S. M. Jetten and M. Strous, *Nature*, 2006, **440**, 918–921.
43 M. Dos Santos Afonso and W. Stumm, *Langmuir*, 1992, **8**, 1671–1675.
44 S. Peiffer, M. Dos Santos Afonso, B. Wehrli and R. Gaechter, *Environ. Sci. Technol.*, 1992, **26**, 2408–2413.
45 L. Holmkvist, T. G. Ferdelman and B. B. Jørgensen, *Geochim. Cosmochim. Acta*, 2011, **75**, 3581–3599.

46 R. C. Aller and P. D. Rude, *Geochim. Cosmochim. Acta*, 1988, **52**, 751–765.
47 D. R. Lovley and E. J. P. Phillips, *Appl. Environ. Microbiol.*, 1994, **60**, 2394–2399.
48 W. Yao and F. J. Millero, *Mar. Chem.*, 1996, **52**, 1–16.
49 J. Zopfi, M. E. Böttcher and B. B. Jørgensen, *Geochim. Cosmochim. Acta*, 2008, **72**, 827–843.
50 P. Anschutz, B. Sundby, L. Lefrançois, G. W. Luther Iii and A. Mucci, *Geochim. Cosmochim. Acta*, 2000, **64**, 2751–2763.
51 B. Deflandre, A. Mucci, J.-P. Gagné, C. Guignard and B. j. Sundby, *Geochim. Cosmochim. Acta*, 2002, **66**, 2547–2558.
52 F. C. Van Duyl, W. Van Raaphorst and A. J. Kop, *Mar. Ecol.: Prog. Ser.*, 1993, **100**, 85.
53 R. Bartlett, R. J. G. Mortimer and K. Morris, *Chem. Geol.*, 2008, **250**, 29–39.
54 J.-C. Clément, J. Shrestha, J. G. Ehrenfeld and P. R. Jaffé, *Soil Biol. Biochem.*, 2005, **37**, 2323–2328.
55 S. Hulth, R. C. Aller and F. Gilbert, *Geochim. Cosmochim. Acta*, 1999, **63**, 49–66.
56 J. E. Mackin and R. C. Aller, *Limnol. Oceanogr.*, 1984, **29**, 250–257.
57 B. Thamdrup and T. Dalsgaard, in *Microb. Ecol. Oceans*, John Wiley & Sons, Inc., 2008, pp. 527–568, DOI: 10.1002/9780470281840.ch14.
58 D. E. Hammond, J. McManus, W. M. Berelson, T. E. Kilgore and R. H. Pope, *Deep Sea Res., Part II*, 1996, **43**, 1365–1412.
59 W. B. Homoky, D. J. Hembury, L. E. Hepburn, R. A. Mills, P. J. Statham, G. R. Fones and M. R. Palmer, *Geochim. Cosmochim. Acta*, 2011, **75**, 5032–5048.
60 G. W. I. Luther, B. Sundby, B. L. Lewis, P. J. Brendel and N. Silverberg, *Geochim. Cosmochim. Acta*, 1997, **61**, 4043–4052.
61 R. C. Aller, P. O. J. Hall, P. D. Rude and J. Y. Aller, *Deep Sea Res., Part I*, 1998, **45**, 133–165.
62 P. Anschutz, K. Dedieu, F. Desmazes and G. Chaillou, *Chem. Geol.*, 2005, **218**, 265–279.
63 C. Hyacinthe, P. Anschutz, P. Carbonel, J. M. Jouanneau and F. J. Jorissen, *Mar. Geol.*, 2001, **177**, 111–128.
64 J. Tapia and S. Audry, *Appl. Geochem.*, 2013, **31**, 60–78.
65 R. Bartlett, R. J. G. Mortimer and K. M. Morris, *Cont. Shelf Res.*, 2007, **27**, 1501–1509.
66 B. Thamdrup and T. Dalsgaard, *Geochim. Cosmochim. Acta*, 2000, **64**, 4157–4164.
67 T. V. Pogodaeva, T. I. Zemskaya, L. P. Golobokova, O. M. Khlystov, H. Minami and H. Sakagami, *Russ. Geol. Geophys.*, 2007, **48**, 886–900.
68 T. I. Zemskaya, S. M. Chernitsyna, N. M. Dul'tseva, V. N. Sergeeva, T. V. Pogodaeva and B. B. Namsaraev, *Microbiology*, 2009, **78**, 117–124.
69 N. S. Suits and M. A. Arthur, *Deep Sea Res., Part I*, 2000, **47**, 1829–1853.
70 J. Sørensen, *Geomicrobiol. J.*, 1987, **5**, 401–421.
71 K. F. Ettwig, M. K. Butler, D. Le Paslier, E. Pelletier, S. Mangenot, M. M. M. Kuypers, F. Schreiber, B. E. Dutilh, J. Zedelius, D. de Beer, J. Gloerich, H. J. C. T. Wessels, T. van Alen, F. Luesken, M. L. Wu, K. T. van de Pas-Schoonen, H. J. M. Op den Camp, E. M. Janssen-Megens, K.-J. Francoijs, H. Stunnenberg, J. Weissenbach, M. S. M. Jetten and M. Strous, *Nature*, 2010, **464**, 543–548.
72 K. F. Ettwig, S. Shima, K. T. Van De Pas-Schoonen, J. Kahnt, M. H. Medema, H. J. M. Op Den Camp, M. S. M. Jetten and M. Strous, *Environ. Microbiol.*, 2008, **10**, 3164–3173.
73 H. Fossing, V. A. Gallardo, B. B. Jorgensen, M. Huttel, L. P. Nielsen, H. Schulz, D. E. Canfield, S. Forster, R. N. Glud, J. K. Gundersen, J. Kuver, N. B. Ramsing, A. Teske, B. Thamdrup and O. Ulloa, *Nature*, 1995, **374**, 713–715.
74 B. B. Jørgensen and V. A. Gallardo, *FEMS Microbiol. Ecol.*, 1999, **28**, 301–313.
75 B. Thamdrup and D. E. Canfield, *Limnol. Oceanogr.*, 1996, **41**, 1629–1650.
76 R. Dermott and M. Legner, *J. Great Lakes Res.*, 2002, **28**, 688–697.
77 R. Lauterborn, *Ber. Dtsch. Bot. Ges.*, 1907, **25**, 238–242.
78 M. Nishino, M. Fukui and T. Nakajima, *Water Res.*, 1998, **32**, 953–957.
79 N. M. Dul'tseva, S. M. Chernitsina and T. I. Zemskaya, *Microbiology*, 2012, **81**, 67–78.
80 B. B. Namsaraev, L. E. Dulov, G. A. Dubinina, T. I. Zemskaya, L. Z. Granina and E. V. Karabanov, *Microbiology*, 1994, **163**, 193–197.
81 M. G. Prokopenko, M. B. Hirst, L. De Brabandere, D. J. P. Lawrence, W. M. Berelson, J. Granger, B. X. Chang, S. Dawson, E. J. Crane Iii, L. Chong, B. Thamdrup, A. Townsend-Small and D. M. Sigman, *Nature*, 2013, **500**, 194–198.
82 A. W. Mackay, D. B. Ryves, R. W. Battarbee, R. J. Flower, D. Jewson, P. Rioual and M. Sturm, *Global Planet. Change*, 2005, **46**, 281–297.

2.3 A new method to quantify bioavailable elements and mobile ATP on rock surfaces and lichens

Submitted to Chemical Geology

A new method to quantify bioavailable elements and mobile ATP on rock surfaces and lichens

*Natascha T. Torres[ab], Thomas Chwalek[ac], Helen Droz-Georget[c], Beat Müller[a], Helmut Brandl[d], Peter C. Hauser[b] and Gerhard Furrer[c]**

[a] Eawag, Swiss Federal Institute of Aquatic Science and Technology, CH-6047 Kastanienbaum, Switzerland

[b] Department of Chemistry, University of Basel, CH-4056 Basel, Switzerland

[c] Institute of Biogeochemistry and Pollution Dynamics, ETH Zurich, CH-8092 Zürich, Switzerland

[d] Institute of Evolutionary Biology and Environmental Studies, University of Zürich, CH-8057 Zurich, Switzerland

* Gerhard Furrer; Phone: +41 44 633 60 09; email: gerhard.furrer@env.ethz.ch

KEYWORDS. adenosine triphosphate, capillary electrophoresis, granite, lichen, *Rhizocarpon geographicum*

1 ABSTRACT

2 The quantification of mobile ions on rock surfaces is essential for the investigation of mineral
3 weathering. A need for such measurements arises from the study of initial soil formation in
4 pioneering environments, the biogeochemical weathering of monuments and buildings, and the
5 chemical reactivity of minerals in general. In the case of mineral surfaces covered by lichens, the
6 quantification of adenosine triphosphate (ATP) reveals an indication of the vitality of the
7 organisms. To date, non-destructive investigations of rock surfaces and growth of biofilms have
8 generally been limited to visual techniques. We evaluated a new technique for the analysis of
9 readily available ions and ATP. For this, a single drop of pure water is spread on bare mineral
10 surfaces or rock-based crustose lichens. The solution is recollected and analyzed for dissolved
11 ions and ATP using a portable capillary electrophoresis instrument and a luminometer,
12 respectively. By application of the method, we show the natural heterogeneity of available ions
13 on freshly broken granite surfaces and the effects of subsequent wetting, freezing and thawing. In
14 addition, the influence of humidity and age of crustose lichens is demonstrated by ion and ATP
15 analysis.

16 # 1 INTRODUCTION

17 Rock surfaces are habitats for microbes and primary sources of nutrients. The non-destructive
18 investigation of these surfaces and their degradation has been limited to visual techniques. In
19 water-unsaturated conditions, the reactivity of accessible minerals controls the rate of weathering
20 and therefore the rate of initial soil formation and development of soil fertility [1]. This is a
21 prerequisite for the prosperity of life and can influence global climate [2].

To date, the mobilized ions on rock surfaces have been analyzed only indirectly, i.e. via the measurement of the infiltrate [3] or by the weight loss of the rock [4]. The heterogeneity of rock surfaces becomes particularly pronounced on the microscale, the scale of migroorganisms. Weathering processes and the microbial colonization develop at particularly vulnerable sites, such as fissures, grain boundaries, as well as kinks and steps within single minerals [5]. The weathering age of rocks has often been determined by lichens, due to their slow growth and longevity [6]. Nevertheless, metabolic processes can hardly be studied, since the cultivation and separation of crustose lichens is fraught with difficulties [7]. The concentration of adenosine triphosphate (ATP) indicates the viability of the lichens [8 and citations therein], but the analysis has been limited to lichens that can easily be separated from the substrate [e.g.9-11].

The present work introduces a new and non-destructive sampling method for the measurement of readily available ions and mobile ATP from rock surfaces that are either bare or covered by lichens. The method (DoR, "Drop-on-Rock") is based on the analysis of a drop of pure water spread onto and recollected from the rock surface to be investigated. Dissolved ions and ATP are analyzed by a capillary electrophoresis (CE) instrument and a luminometer, respectively. Both instruments are portable and can deal with sample volumes as low as 25 µL.

We applied the DoR method to freshly broken and pre-weathered granite surfaces, as well as to rock surfaces covered by map lichen (*Rhizocarpon geographicum*). In particular, we evaluated (i) the macroscopic surface heterogeneity of bare granite surfaces with respect to readily available cations and (ii) the effect of wetting and freezing. In addition, (iii) we analyzed the readily available ions and mobile ATP on lichens. For this purpose, lichen-covered granite surfaces were investigated with respect to their age (size) and to humidity.

2 EXPERIMENTAL

2.1 Granite samples

All experiments were conducted with granite specimens. Fist-sized samples were collected along the glacier chronosequence of the Damma glacier forefield (Central Alps, Switzerland) from 2012 to 2014. Samples for the lichen experiments were collected in October 2013 and June 2014 using sterile gloves and immediately packed in sterile plastic bags for transportation to the laboratory. From each sampling site, the lichens with the largest diameter were preferred, as they represented the earliest colonization. The investigated granite was composed mainly of plagioclase, quartz, microcline, muscovite, biotite, epidote. Accessory minerals were chlorite, apatite, and magnetite [12-14]. The granite was formed 300 million years ago, metamorphosed under greenschist conditions and belongs to the Aar massif [15, 16].

To obtain pairs of freshly broken and unweathered rock surfaces, the granite samples for the wetting and freezing experiments were cut to ~ 100 cm^3 uniform cuboids or fist-sized chunks using a water-cooled diamond saw. Afterwards, the samples were incised to a depth of 1 cm with the diamond saw, cleaned with pure water, and split with a chisel and a hammer to produce a pair of mirror-imaged specimens. All samples were stored in a clean bench with a high efficiency particulate air filter (HEPA) to avoid contamination. All freshly broken rock surfaces were photographed to document the sampling points.

2.2 Wetting and freezing-thawing experiments

The granite samples were placed in plastic boxes filled with pure water up to 1 cm below the freshly broken surface for the duration of six hours. Care was taken not to submerge the surface to be sampled in water to avoid the removal of readily available ions. The assembly was placed in a desiccator (without drying agent) and a vacuum applied causing the pore spaces of the granite

67 sample to fill with water, thus humidifying the granites completely. The water-saturated granite
68 specimen were either stored in the clean bench for drying or frozen at -20 °C for 24 hours. For
69 thawing, the granite samples were placed back into the clean bench at room temperature for
70 another 24 hours. As soon as the granite specimens were visibly dry the next DoR sampling was
71 carried out. The same spots were sampled before and after wetting and freezing.

72 2.3 Field exposure experiments on Mount Pilatus

73 Freshly broken granite surfaces (6 pairs of mirror-faced samples) were exposed on three field
74 locations within an altitude transect on the northern slope of Mount Pilatus, Central Switzerland.
75 The lowest location (1007 m a.s.l.) was in a fen characterized by low-grown vegetation. The
76 intermediate location (1445 m a.s.l.) was in a forest glade and the topmost location was above the
77 timberline on the roof of the hotel building on top of Mount Pilatus (2075 m a.s.l.) (Figure 1,
78 left). At all sites, humidity and temperature were recorded with a sensor (Hioki LR5001, Nagano,
79 Japan). Additional climate data were provided by the Federal Office of Meteorology and
80 Climatology (IDAWEB 1.1.21© MeteoSwiss). For the study of the influence of atmospheric
81 deposition both halves of the fist-sized granite chunks were mounted side by side. One half of
82 each pair was positioned facing downwards, while the corresponding half was placed facing
83 upwards in open plastic containers (17 x 25 cm) with holes drilled for drainage. Inside the
84 containers the rock samples were suspended with the help of a grid made from cable ties
85 (Figure 1, right). The plastic containers exposed below the timberline were mounted 40 cm above
86 ground to avoid soil contamination. DoR samples were taken on site from 2012 to 2014 once
87 each summer.

2.4 DoR sampling on lichens and ATP analysis

Lichen-covered granite samples from 2013 were stored in plastic bags at 5 °C, while those from 2014 were placed on the roof of the institute but sheltered to avoid atmospheric deposition. The humidity experiments were conducted with samples from 2013, all other experiments with samples from 2014.

Before sampling, all rocks collected in 2014 were conditioned in a self-built humidifier system (plastic box of 16 x 39 x 68 cm, containing an automatic humidifier from Le Veil, Spokane, WA, USA) for 0.5 hours with 80% humidity. Note, DoR sampling on lichens was carried out without the ring of rubber foam as the surface of lichens is hydrophobic the drop remained confined. The age of the lichens was derived from their diameter assuming an annual growth rate of 0.5 mm [17, 18]. ATP analysis was performed with the BacTiter-Glo Microbial Cell Viability Assay and the GloMax® 20/20 luminometer (Promega, Dübendorf, Switzerland). The ATP for the stock solution was from Thermo Scientific (Waltham, MA, USA). In deviation from the standard procedure given in the manual of the instrument the assay kit was equilibrated at room temperature and 10 mL of the substrate added to the buffer to prepare the reagent. The reagent (30 µL) was then pipetted into sterile reaction tubes (Greiner Bio One, Frickenhausen, Germany) and stored at -20 °C for further use. Samples and reagents were warmed up to 25 °C for 2 minutes. For the actual measurement, 30 µL of the sample was added to the reagent solution and incubated at 25 °C for 20 seconds.

2.5 Ion analysis with capillary electrophoresis

The analysis of ions was performed with a portable CE instrument with capacitively coupled contactless conductivity detection (C^4D) [19, 20]. The equipment can deal with ~25 µL of sample and is suitable for field applications [21]. The detailed measurement protocol is described in Torres et al. [22] In short, the background electrolyte solution consisted of 11 mmol/L L-histidine,

112 50 mmol/L acetic acid, and 1.5 mmol/L 18-crown-6. Reagents for the stock solutions were
113 provided by Fluka or Sigma-Aldrich (Buchs, Switzerland; Steinheim, Germany). Pure water for
114 the preparation of the solutions and for the DoR sampling was from Merck (Zug, Switzerland).
115 Vials and pipette tips were cleaned with 0.1 molar acetic acid and pure water, and air dried in a
116 HEPA clean bench. A fused silica capillary (50 µm i.d., 360 µm o.d., 55 cm length) (BGB
117 Analytic AG, Böckten, Switzerland) was used for the separation of ions under application of a
118 voltage of 15 kV. For the simultaneous analysis of anions and cations, we injected the sample on
119 two different CE instruments (identical set-ups, but different polarities) for 20 seconds
120 hydrodynamically with 15 cm height for anions and 8 cm height for cations. The TraceDec® C^4D
121 detector (Innovative Sensor Technologies, Strasshof, Austria) and the eDAQ Chart software
122 (version 5.5.8, Denistone East NSW 2112, Australia) were employed for data acquisition. The
123 statistical significance of the data was evaluated with the Student's t-test in R (GNU statistical
124 software).

125 ## 2.6 Scanning electron microscopy (SEM)

126 Scanning electron microscopy (Nova NanoSEM 230 FEI) with a gaseous analytical detector
127 (GAD) was used for the visualization of the surface topography of the granite samples before and
128 after freezing and thawing. To avoid alteration of the rock surfaces, the samples were not coated
129 and a low vacuum mode was chosen (0.7 mbar). The spot size was set to 3.5, and beam current to
130 15 kV. The rock surfaces were marked with three dots (~0.25 mm) of colloidal silver paste
131 (Electron Microscopy Sciences, Hatfield, USA) as anchor points of a coordinate system.

Figure 1. Experimental setting of exposed rock samples located at the hotel on top of Mount Pilatus (Central Switzerland). On the right, a pair of freshly broken mirror-faced granite surfaces is visible in the box. One surface was facing upwards (back) and the other was facing downwards (front) to determine the influence of atmospheric deposition. A humidity and temperature sensor was mounted in front of the box.

3 RESULTS AND DISCUSSION

3.1 The drop-on-rock method

The extraction of readily available ions in a small volume (50 µL) of water from bare rock surfaces required its confinement in a defined area. We used a ring made of rubber foam (ear plugs) of clinical quality (Ohropax, Wehrheim, Germany) with an inner diameter of 8 mm. The rubber foam proofed to be chemically inert to the species of interest and allowed easy handling without leaking. While pipetting, the rubber ring was pressed onto the rock surface using a plastic

145 ring as shown in Figure 2 (left). The contact time between the rock and the drop was set as short
146 as possible (~1 s) as otherwise the water drop would be absorbed by the pores of the granite
147 samples. The procedure was repeated two times for each sample spot with the same drop of water
148 to guarantee a sufficient mixing. Finally, the remaining solution (~30 µL) was transferred to a
149 100 µL plastic vial or a sterile 2 mL reaction tube (Greiner Bio One, Frickenhausen, Germany)
150 for the ion or ATP analysis, respectively.

151 Various eluents were tested to assure that only readily available ions were extracted but not
152 ions released from the crystal lattice by hydrolysis. The differences in ion concentrations
153 removed from the surface with a drop of pure H_2O, 1 mmol/L HCl, or 1 mmol/L oxalic acid were
154 statistically not significant. Hence, we conclude that the contact time of a few seconds was short
155 enough to avoid hydrolysis. Repeated sampling of one spot resulted in decreasing concentrations
156 of ions removed from the surface. This behavior suggested that the surface was increasingly
157 exhausted of readily available compounds as a result of stepwise elution.

158 The portable CE instrument allowed the ion analysis of tiny sample volumes (~25 µL) within
159 10 minutes with detection limits in the sub-micromolar range [22]. The quality of the sampling
160 water was critical for low detection limits. For the analysis of mobile ATP with the luminometer
161 we achieved standard deviations of $< 10\%$ for concentrations of ≤ 5 nmol/L, and $< 5\%$ for
162 concentrations of ≤ 10 nmol/L from triplicate measurements. Relative standard coefficients for
163 five point calibration curves were $\geq 99\%$.

Figure 2. Left: Applying the DoR method on a freshly broken rock surface with the confining rubber foam ring (yellow) pressed on by a plastic ring (colorless, opaque). Right: Applying the DoR method on *R. geographicum* growing on a granite specimen. Note that the drop at the pipette tip remains intact due to the hydrophobic nature of the surface of the lichen.

3.2 Ion availability from freshly broken and water-treated granite surfaces

The release of ions from a rock surface is expected to depend on its mineral composition, the orientation of the minerals in relation to the rock's surface, and its weathering state [e.g. 23]. Therefore, ion availability was tested at selected spots on the rock surface at areas dominated by either quartz or biotite minerals. Measurements were made first on the untreated surface after break-up and repeated after wetting and drying of the rock. The photo in Figure 3 shows one face of a cuboid granite specimen with the investigated DoR sampling spots. Initial measurements on untreated surfaces did not display any significant difference between locations dominated by either quartz or biotite. While quartz is prone to be most resistant with regard to weathering, e.g.

biotite (Spots # 1 and 3, Figure 3) and feldspar contain ions that can easily be removed from the crystal lattice by hydrolysis. Results indicated that no dissolution of surface minerals occurred on freshly broken surfaces. However, granite surfaces that had been subjected to six hours of wetting, followed by drying, before sampling showed that all ion concentrations significantly increased. Concentrations were highest on spots dominated by biotite minerals (# 3, 1) and decreased with increasing proportions of quartz (in the sequence of # 4, 2, 5). The results were confirmed with replicate tests on three different granite surfaces (data not shown).

In conclusion, wetting caused a correlation between the concentrations of the released ions and the weatherability of the sampled spots.

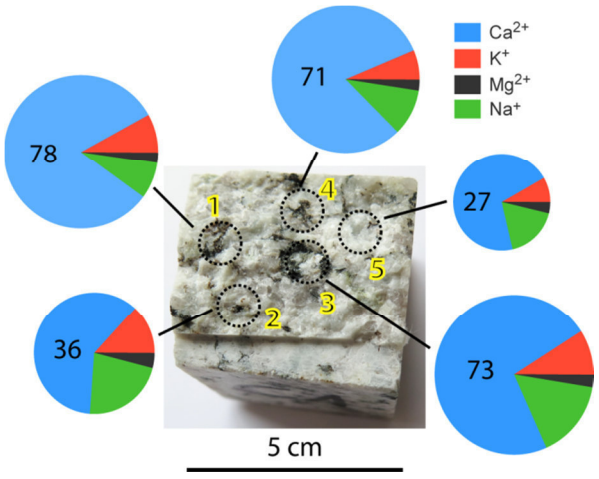

Figure 3. Freshly broken surface of a granite cuboid exhibiting a typical mineral distribution. Dashed circles highlight the areas sampled with the DoR method. Pie charts represent the cation concentrations on the sampled spots. Calcium concentrations (µmol/L) are indicated in the blue parts of the pie charts.

3.3 Ion availability from frozen and thawed granite surfaces

To investigate the impact of physical stress several pairs of mirror-imaged granite specimens were treated by freezing and thawing. Figure 4 shows a surface of a granite specimen with the

196 investigated DoR sampling spots (top) and the sodium concentrations in the DoR samples before
197 and after several freeze-thaw cycles (bottom). Regardless the increasing number of freeze-thaw
198 cycles the concentrations did not show any trend. The scatter of data along the number of freeze-
199 thaw cycles were probably caused by slight deviations of the sampled surface area in the course
200 of the experimental campaign. As seen already in section 3.2, the DoR samples from spots
201 dominated by feldspar or biotite (# 1, 2, and 3) generally released higher sodium concentrations
202 than other spots.

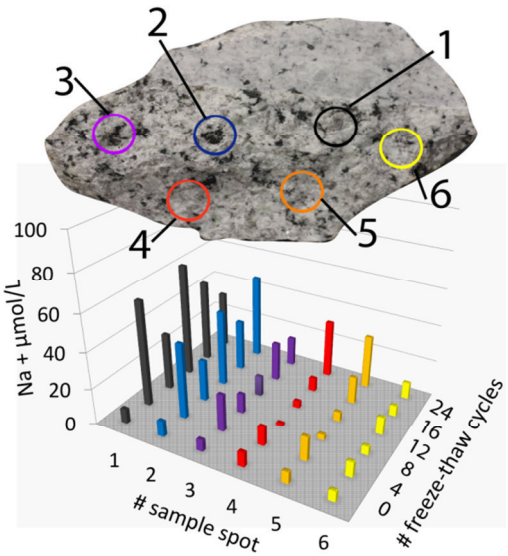

203

204 **Figure 4**. Sodium concentrations obtained from sampling spots 1 - 6 after various cycles of
205 freezing and thawing (0, 4, 8, 12, 16, 24). Sampling Spot # 1 was characterized by a high content
206 of feldspar minerals, while 2 and 4 contained more biotite. Spots # 3, 5 and 6 were dominated by
207 quartz.

208 In addition, we compared a pair of mirror-imaged granite specimens, one only wetted, and the
209 other also frozen and thawed. The surfaces of both halves released more ions than before
210 treatment - surprisingly at comparable concentrations. To examine the possibility of surface
211 generation through freezing, the same 300 µm x 300 µm surface area before and after freezing

and thawing was imaged by SEM (Figure 5). As a consequence of frost action, pronounced surface break-down and rearrangement of particles were observed. However, the expected increase of instantly available cations was not confirmed by the CE measurements. Thus, the mobilization of cations from the granite surface appears to be promoted mainly by wetting rather than by subsequent freezing and thawing.

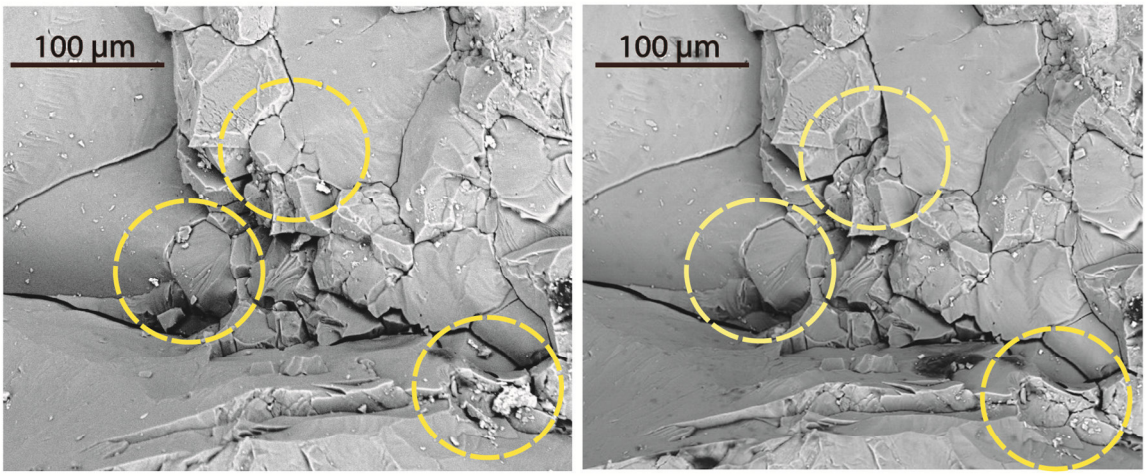

Figure 5. SEM pictures of feldspar minerals on a granite surface before (left) and after (right, slightly distorted with respect to the left image) freezing and thawing. The yellow circles highlight altered locations, where material was quarried out or rearranged. (An animation of surface changes due to freezing are provided in the supplementary information).

Again, surface spots dominated by phyllosilicates showed the highest concentrations of instantly available cations after wetting. Frost action did not increase the availability of ions in our experiments. Hence, the creation of new reactive surfaces relevant for the instant availability of cations appears to depend on the scale. Additional alterations on the micrometer scale through freezing and thawing are probably not relevant for increasing the release of ions during the very beginning of exposure. To verify these laboratory results we exposed granite samples to alpine field conditions (section 3.4).

3.4 Ion availability from rocks exposed to an alpine environment

We investigated the influence of atmospheric deposition and altitude-dependent climate on the surface-specific availability of nutrients in an alpine environment. Fresh granite surfaces were exposed on the northern slope and on top of Mount Pilatus from 2012 to 2014. On the mountain top, the temperature ranged from -25 °C to +55 °C. In contrast, the temperature at the lowest exposure site that was surrounded by shrub-sized vegetation, varied only between -5 °C and +22 °C. Among the approximately 200 DoR samples, no significant differences were found between the different altitudes. This applied also to the comparison between granite surfaces that were facing upwards or downwards.

At all three altitudes, the concentrations of phosphate, nitrate and sulfate were mostly below detection limits according to Torres et al. [22]. However, less than 10 % of the DoR samples collected on the upwards oriented granite surfaces showed concentrations of phosphate, nitrate and sulfate in the order of 1-40, 0.5-10, and 0.5-5 µmol/L, respectively. Annual rates of atmospheric deposition were several orders of magnitude higher [24]. Thus, we conclude that bare granite surfaces did not accumulate atmospheric deposition, and therefore the DoR samples include the recently deposited material only. This can be seen also in the comparison of the three years of exposure, i.e. the highest ion concentrations were observed during the driest summer (2013).

In conclusion, the contribution of atmospheric deposition is of limited residence time, if at all. For the given time-span, extrinsic factors such as frost, wind and radiation did not enhance the reactivity of the granite surface. These findings are in agreement with the freeze-thaw experiments (previous chapter). Despite the resistance of granite with respect to extrinsic factors, concentrations of instantly available ions can be significantly increased after the first contact with water - especially on spots with minerals prone to weathering.

3.5 ATP and cation availability from lichen surfaces

The lichen *R. geographicum* is one of the first colonizers of freshly exposed rocks. Within the same locality under identical climatic conditions the lichens' diameter is seen to represent their relative age [6]. Although, *R. geographicum* is widely used for geochronology, the study of crustose lichens is challenging as they grow very slowly and cannot be seperated easily from the substrate [7]. Although, ATP represents the vitality of the lichen [9], the analysis of ATP has not been applied yet to crustose lichen.

Using the DoR method we analyzed in parallel the concentrations of ions and mobile ATP as a factor of humidity and age (size). As shown in Figure 6 (left panel), initial experiments revealed that the mobile ATP on a lichen surface was highly dependent on ambient humidity. Mobile ATP was significantly higher when lichens were conditioned with moisture in comparison to unconditioned lichens. Thus, the production of ATP was reduced if the relative humidity was not optimal. Lichens are able to constrain their metabolism to protect themselves from desiccation [18]. To study the necessary time span of humidification for optimal metabolic rates, we analyzed the ATP concentrations of three individuals as a function of their exposure time (0.5, 2, and 13 hours) to a constant ambient humidity of 80%. The data shown in Figure 6 (right) reveal that ATP did not increase further after the first half hour of humidification.

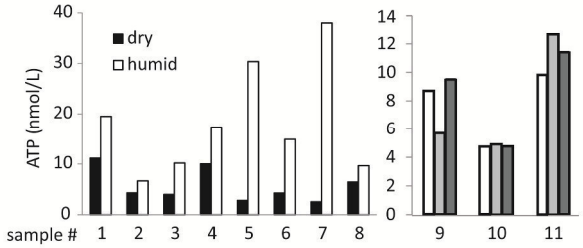

Figure 6. Left: Immediately mobile ATP on dry and humid lichens. Right: Effect of humidification time (80% humidity) on ATP availability after 0.5 h (white), 2 h (light grey) and 13 h (dark grey). The data represent single measurements.

Furthermore, we investigated the relationship of the lichens' size and mobile ATP to estimate the dependence of vitality on age. ATP concentrations measured from *R. geographicum* individuals of 0.5 to 3.9 cm in diameter (10 to 80 years old) indicate a parabolic trend (Figure 7). Our findings are in accordance with previous observations of Armstrong and Bradwell [7, 25]. Their data on radial growth rates of 3 to 50 years old lichens showed also a parabolic trend. Therefore, they concluded that growth accelerates after colonization and decelerates as lichens become older. It is assumed that cell degradation in the senescent phase may slow down growth [26]. This could also explain the decline in ATP concentration in our study. It must be stated, however, that differences in ATP availability from the older part (center) in comparison to the younger part (corona) of *R. geographicum* were not statistically significant.

The analysis of potassium in the same DoR samples revealed a similar parabolic trend as observed from ATP. However, the other prominent cations, i.e. sodium, calcium and magnesium did not show any trend as a function of size. Potassium is an important nutrient for the lichen's algae and can be mobilized by lichens from biotite [27,28]. To date it is not clear if a limited supply of K^+ for the algae cell is corresponding to cell degradation. The DoR method may be a useful tool to study such metabolic interactions**.**

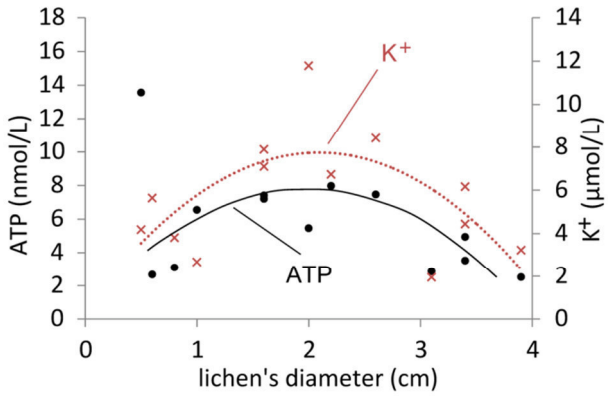

Figure 7. The dependence of mobile ATP (black dots) and readily available K^+ (red crosses) on thallus size of *R. geographicum*. Data points are representing mean values of four DoR samples. Curves show best fit (the outlier of 14 nmol/L ATP was omitted for the fitting).

In conclusion, the DoR method proved to be applicable for the investigation of rock surfaces for their readily available ions and mobile ATP. This opens a new experimental access to surface processes. The sampling procedure is simple, non-destructive and therefore also ideal for on-site studies, especially in remote areas or on samples that cannot be removed, e.g. buildings, monuments or large boulders. The analysis with the portable capillary electrophoresis instrument and the luminometer is reliable, inexpensive and suitable for fieldwork. A promising future application might be the investigation of microorganisms in interaction with their chemical environment, e.g. by identifying the enrichment of elements on surfaces. As a follow-up to this study, the initial weathering of further rock types will be investigated with the DoR method, e.g. limestone, which is a very common building material and also important in global weathering cycles.

Appendix A.

A video animation of SEM pictures shows granite surfaces before and after freezing and thawing. This material can be found online at

Acknowledgements

We are grateful for technical support by Beat Kienholz, Michael Schurter (both eawag), and Pius Dahinden (Pilatus-Bahnen AG). For the analytical support we thank Brian Sinnet, who helped with the scanning electron microscope and Frederic Hammes, who shared his experiences in the analysis of ATP (both eawag). Furthermore, we thank Monika Niederhuber and Daniel Trüssel (both ETH Zürich) for the video animation of the SEM pictures. The authors acknowledge support by the Swiss National Science Foundation (Grant no. 200021-137715).

Abbreviations

ATP adenosine triphosphate, CE capillary electrophoresis, C4D capacitively coupled contactless conductivity detection, SEM scanning electron microscopy

References

(1) Flemming, H.-C.; Wingender, J. The biofilm matrix. *Nat. Rev. Microbiol.* **2010,** *8* (9), 623-633.

(2) Paytan, A. Mountains, Weathering, and Climate. *Science* **2012,** *335* (6070), 810-811.

(3) Zhu, B.; Wang, T.; You, X.; Gao, M.-R. Nutrient release from weathering of purplish rocks in the Sichuan Basin, China. *Pedosphere* **2008,** *18* (2), 257-264.

(4) Yokoyama, T.; Matsukura, Y. Field and laboratory experiments on weathering rates of granodiorite: Separation of chemical and physical processes. *Geology* **2006,** *34* (10), 809-812.

(5) Brehm, U.; Gorbushina, A.; Mottershead, D. The role of microorganisms and biofilms in the breakdown and dissolution of quartz and glass. *Palaeogeogr. Palaeocl.* **2005,** *219* (1), 117-129.

(6) Beschel, R. E. *Dating rock surfaces by lichen growth and its application to the glaciology and physiography (Lichenometry)*; University of Toronto Press: Toronto, 1961.

(7) Armstrong, R.; Bradwell, T. Growth of crustose lichens: a review. *Geogr. Ann. A.* **2010,** *92* (1), 3-17.

(8) Conti, M.; Cecchetti, G. Biological monitoring: lichens as bioindicators of air pollution assessment—a review. *Environ. Pollut.* **2001,** *114* (3), 471-492.

(9) Kardish, N.; Ronen, R.; Bubrick, P.; Garty, J. The influence of air pollution on the concentration of ATP and on chlorophyll degradation in the lichen, Ramalina duriaei (De Not.) Bagl. *New phytol.* **1987,** *106* (4), 697-706.

(10) Garty, J.; Kardish, N.; Hagemeyer, J.; Ronen, R. Correlations between the concentration of adenosine tri phosphate, chlorophyll degradation and the amounts of airborne heavy metals and sulphur in a transplanted lichen. *Arch. Environ. Con. Tox.* **1988,** *17* (5), 601-611.

(11) Silberstein, L.; Siegel, B.; Siegel, S.; Mukhtar, A.; Galun, M. Comparative studies on Xanthoria parietina, a pollution resistant lichen, and Ramalina duriaei, a sensitive species. I. Effects of air pollution on physiological processes. *The Lichenologist* **1996,** *28* (04), 355-365.

(12) Deer, W. A.; Howie, R. A.; Zussman, J. *An introduction to the rock-forming minerals*; Longman: London, 1992.

(13) Frey, B.; Rieder, S. R.; Brunner, I.; Plötze, M.; Koetzsch, S.; Lapanje, A.; Brandl, H.; Furrer, G. Weathering-associated bacteria from the Damma glacier forefield: physiological capabilities and impact on granite dissolution. *Appl. Environ. Microb.* **2010,** *76* (14), 4788-4796.

348 (14) Wongfun, N.; Götze, J.; Furrer, G.; Brandl, H.; Plötze, M. Effect of water regime and
349 vegetation on initial granite weathering in a glacier forefield: Evidences from CL, SEM, and
350 Nomarski DIC microscopy. *Geoderma* **2013,** *211*, 116-127.

351 (15) Bernasconi, S. M.; Bauder, A.; Bourdon, B.; Brunner, I.; Bünemann, E.; Chris, I.;
352 Derungs, N.; Edwards, P.; Farinotti, D.; Frey, B. Chemical and biological gradients along the
353 Damma glacier soil chronosequence, Switzerland. *Vadose Zone J.* **2011,** *10* (3), 867-883.

354 (16) Schaltegger, U. The Central Aar granite: highly differentiated calc-alkaline magmatism in
355 the Aar Massif (Central Alps, Switzerland). *Eur. J. Mineral.* **1990**, 245-260.

356 (17) Proctor, M. Sizes and growth-rates of thalli of the lichen Rhizocarpon geographicum on
357 the moraines of the Glacier de Valsorey, Valais, Switzerland. *The Lichenologist* **1983,** *15* (03),
358 249-261.

359 (18) Henssen, A.; Jahns, H. M.; Santesson, J. *Lichenes: eine Einführung in die Flechtenkunde*;
360 G. Thieme: Stuttgart, 1974.

361 (19) Kubáň, P.; Reinhardt, M.; Müller, B.; Hauser, P. C. On-site simultaneous determination of
362 anions and cations in drainage water using a flow injection-capillary electrophoresis system with
363 contactless conductivity detection. *J. Environ. Monit.* **2004,** *6* (3), 169-174.

364 (20) Kubáň, P.; Nguyen, H. T. A.; Macka, M.; Haddad, P. R.; Hauser, P. C. New fully portable
365 instrument for the versatile determination of cations and anions by capillary electrophoresis with
366 contactless conductivity detection. *Electroanal.* **2007,** *19* (19), 2059-2065.

(21) Torres, N. T.; Och, L. M.; Hauser, P. C.; Furrer, G.; Brandl, H.; Vologina, E.; Sturm, M.; Bürgmann, H.; Müller, B. Early diagenetic processes generate iron and manganese oxide layers in the sediments of Lake Baikal, Siberia. *Env. Sci. Process. Impact.* **2014,** *16* (4), 879-889.

(22) Torres, N. T.; Hauser, P. C.; Furrer, G.; Brandl, H.; Müller, B. Sediment porewater extraction and analysis combining filter tube samplers and capillary electrophoresis. *Env. Sci. Process. Impact.* **2013,** *15* (4), 715-720.

(23) Bisdom, E.; Stoops, G.; Delvigne, J.; Curmi, P.; Altemuller, H. Micromorphology of weathering biotite and its secondary products. *Pedologie* **1982,** *32* (2), 225-252.

(24) Furrer, G.; Sollins, P.; Westall, J. C. The study of soil chemistry through quasi-steady-state models: II. Acidity of soil solution. *Geochim. Cosmochim. Ac.* **1990,** *54* (9), 2363-2374.

(25) Armstrong, R. A. Growth curve of the lichen Rhizocarpon geographicum. *New phytol.* **1983,** *94* (4), 619-622.

(26) Armstrong, R. A.; Smith, S. Factors associated with degeneration of the thallus centre in foliose lichens. *Symbiosis* **1997,** *22* (3), 293-302.

(27) Lee, M.; Parsons, I. Biomechanical and biochemical weathering of lichen-encrusted granite: textural controls on organic–mineral interactions and deposition of silica-rich layers. *Chem. Geol.* **1999,** *161* (4), 385-397.

(28) Silva, B.; et al. Deteriorative effects of lichens on granite monuments. In *Biodeterioration of stone surfaces*; St. Clair, L., Seaward, M., Eds.; Springer: Netherlands 2004; pp 69-7.

3 Conclusion and Outlook

3.1 Main findings

A new protocol for the extraction and analysis of (i) pore water from lake sediments and (ii) available ions and adenosine triphosphate on rock surfaces and lichens was developed and applied.

Pore water was extracted with filter tube samplers and subsequently analyzed with CE. Major inorganic anions and cations - including Mn(II) and Fe(II) - were fully separated in less than 15 minutes. Sediment pore water was sampled with high spatial resolution, minimal disturbance and without subsequent acidification or dilution. The complex biogeochemistry of Lake Baikal sediments was explained by applying the new method. With on-site measurements in improvised laboratories on the shore of Lake Baikal, the method was proven reliable even when conditions were challenging. Therefore, the risk of sample alteration due to long and laborious transport was minimized.

Furthermore, a new technique (DOR) for the quantification of available ions and ATP on rock surfaces was developed and applied on a granite surface. The spatial heterogeneity of a bare granite surface was shown and the effect of wetting and freezing and thawing was investigated. ATP from crustose lichens that overgrow the rock was found to be highly dependent based upon their age and humidity.

3.2 Main advantages

Conclusively, the study could be performed due to the main advantages of CE, namely that the device is portable and simple and the process from sampling until analysis is rapid. Beside this, CE only requires a few microliters of sample volume.

The CE instrument is portable, lightweight and can be operated by batteries. It fits in a normal-sized backpack or can be transported as hand luggage in air planes. Laborious and heavy sample transport and pretreatment can be avoided by on-site measurements, as the study on Lake Baikal showed. Thus, maximum freedom in decision-making for further sampling is possible at any time, which can be extremely important in remote and hard-to-reach areas. The portability of the CE instrument also allows the application of the DOR method on immobile surfaces, such as buildings, monuments and large boulders. To our knowledge, there were no previous possibilities to study such surfaces, besides through visual assessments.

The rapidity in sampling and subsequent measurements minimizes the risk of sample alteration, e.g. by oxygen and temperature changes, while it enables measuring redox sensitive Fe(II) and phosphate, which is prone to precipitate. Through the analysis of Fe(II) in Lake Baikal sediments, sharp redox boundaries could be determined.

The device is simple and can easily be reproduced. A second CE instrument was built during this study for the simultaneous measurement of anions and cations. The simplicity facilitates a high degree of freedom in handling. The sample injection by siphoning is flexible in duration and height, effective and the total capillary length can be easily adapted, as well as the applied electrical field. Thus, the measurement protocol can be spontaneously refined, e.g. in case of peak overlap resulting from unexpected high concentrations.

Given that only a small sample volume is needed for the analysis, pore water could be extracted fast and with high resolution from sediments. A drop of water - spread on a rock surface to collect available ions - was sufficient for analysis. This application implies that CE is a perfect method for the analysis of interstitial water in general, as well as any kind of aqueous sample that is too small in volume and/or low in concentration to be diluted. By using the filter tube samplers, all water containing sediments or soils can be investigated in mm resolution.

3.3 Main challenges

Despite such advantages, some parts of CE remain challenging. For instance, the analysis of small volumes or low concentrated samples required a number of precautions to avoid contaminations by alkali and alkaline earth ions. All vials, tubes, syringes and pipette tips had to be cleaned with pure water before usage, dried in a clean bench and transported only in sterile plastic bags. However, the risk of sample contamination could not be generally eliminated, especially during field sampling with the DOR method. In general, contaminations were indicated by an unusually high concentration of ammonia, potassium and sodium, while calcium and magnesium both remained in the order of the expected sample concentration. The quality of pure water and buffer solution was critical for high sensitivity and low detection limits.

Temperature changes caused shifts in migration time and sensitivity. Although the detector cell was found to be sufficiently isolated, the buffer solution was adjusting to ambient temperature and thus it was subject to local fluctuations. Thus, periodic calibration measurements were essential.

3.4 Future applications

Recent projects have already been motivated by this work. The mineralization process of organic matter in lake sediments is studied at eawag by using the introduced sampling and measurement protocol for pore water analysis. Although the analysis works well, the procedures are time-consuming for high numbers of samples. Therefore, an automation for the injection of small sample volumes has recently been introduced [1]. Another research project will assess the impacts of mines on aquatic environments in the Andes, whereby the CE instrument will also be modified for this purpose. Both examples show that the high flexibility in design and modes of the CE instrument can be used for versatile projects in the environment. Each new application will define the requirements for the construction of the instrument and the measurement protocol, which

demands experience in handling and technical knowledge. In general, the automation of the system will facilitate routine use, as well as reducing flexibility. The effort in troubleshooting will be greater and should be considered in remote areas, for instance. The remaining question is thus how to make portable CE more user-friendly. Due to the general simplicity and inexpensiveness of the device, low-income countries without access to laboratories could benefit from it. Solutes and surfaces could be assessed for quality or toxicity with a minimum sample volume and effort for analysis. Given that surface analysis with the DoR method is still at the beginning, potentials and limitations for such projects have to be thoroughly investigated in future projects.

References

1 Sáiz, J., Koenka, I. J., García-Ruiz, C., Müller, B., Chwalek, T. & Hauser, P. C. Micro-injector for capillary electrophoresis. *Electrophoresis* (2015).